AFIT/GAP/ENP/97-D-08

DISPLACEMENT OF THE EARTH'S BOW SHOCK
AND MAGNETOPAUSE DUE TO AN IMPINGING
INTERPLANETARY SHOCK WAVE

THESIS

William A. Olson, Captian, USAF

AFIT/GAP/ENP/97D-08

Approved for public release; distribution unlimited

19980127069

DISPLACEMENT OF THE EARTH'S BOW SHOCK AND MAGNETOPAUSE DUE

TO AN IMPINGING INTERPLANETARY SHOCK WAVE

THESIS

Presented to the Faculty of the Graduate School of Engineering Physics

of the Air Force Institute of Technology

Air University

Air Education and Training Command

In Partial Fulfillment of the Requirements for the

Degree of Master of Science in Physics
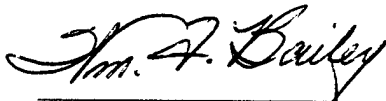
William A. Olson, B.S., M.A.S,

Captain, USAF

December 1997

AFIT/GAP/ENP/97D-08

DISPLACEMENT OF THE EARTH'S BOW SHOCK AND MAGNETOPAUSE

DUE TO AN IMPINGING INTERPLANETARY SHOCK WAVE
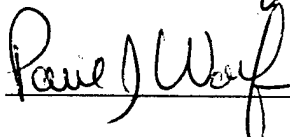
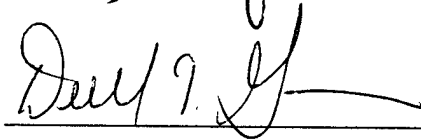William A. Olson, B.S., M.A.S.
Captain, USAF

Approved:

_____
Chairman

26 Nov 97
date

_____

26 Nov 97
date

_____

26 Nov 97
date

ii

<u>Acknowledgments</u>

Table of Contents

List of Figures

List of Tables

Abstract

Interplanetary shock waves (ISWs) propagating through the solar wind can "collide" with the earth's bow shock, resulting in a series of new shocks, contact discontinuities, and rarefaction waves which interact to effectively move the bow shock and magnetopause toward the earth. A one-dimensional MacCormack predictor-corrector algorithm with Flux Corrected Transport (FCT) was developed to model the ISW-bow shock and magnetopause interactions, and to numerically predict their propagation speeds after collision. Analytic relationships for the Mach numbers and propagation speeds of the generated shock waves and contact discontinuities were used to validate the model predicted propagation speeds of the moving bow shock to within five percent of the analytical solutions. Propagation speeds of the moving magnetopause were also determined to within five percent for the gas-dynamic case.

DISPLACEMENT OF THE EARTH'S BOW SHOCK AND MAGNETOPAUSE DUE TO AN IMPINGING INTERPLANETARY SHOCK WAVE

I. Introduction

1.1 Problem Statement

Predict and evaluate bow shock and magnetopause motion resulting from the interaction of an Interplanetary Shock Wave (ISW) with the earth's magnetosheath system using a one dimensional solution of the gas-dynamic and magnetohydrodynamic (MHD) equations.

1.2 Importance of Research

Rapid, large scale movement of the earth's magnetopause generates strong electric fields that accelerate charged particles to high energies, forming regions of enhanced energetic particle concentrations within the magnetosphere. When the displacement of the magnetopause is large enough to bring it within approximately six earth radii then satellites in geosyncronous orbits are directly exposed to energetic solar wind particles. Increased densities of high energy particles in the near-earth environment have damaged military and commercial satellites, caused widespread radio and satellite communications blackouts, and have caused power outages on earth. The ability to predict magnetopause motion resulting from the interaction of an ISW with the earth's magnetosheath system would be a valuable input for computer models used to forecast changes in ion and electron densities in the near-earth environment. Ion and electron

density forecasts based on magnetopause motion would, in turn, be used by operators to reduce the risk of damaging expensive and strategically important satellite systems, and by communicators to manage communications outages caused by changes in the space environment.

This thesis is especially relevant at this time because of the placement of the Solar and Heliographic Observation (SOHO) satellite into a halo orbit about the L1 point upstream in the solar wind on February 14, 1996 (SOHO home page, 1997). From its position upstream in the solar wind, the SOHO satellite is able to provide density, temperature, and velocity measurements about an hour before disturbances in the solar wind reach the earth. Using data from SOHO and methods developed in this thesis, space forecasters will be able to determine an initial estimate of magnetopause motion due to ISW collision with the earth's bow shock in advance of the actual event.

1.3 Scope and Limitations

This thesis will investigate the problem of bow shock and magnetopause motion resulting from the interaction of an interplanetary shock wave impinging on the earth's magnetosheath system. The analysis is restricted to one dimension. Magnetic fields are assumed to be perpendicular to the gas flow and in the z-direction so that slow and intermediate magnetosonic shocks are eliminated from consideration (Parks, 1991,418). The difficulties associated with a kinetic approach are avoided in favor of two fluid models: a gas-dynamic, ideal fluid approximation in which the magnetic field is neglected, and a magnetohydrodynamic fluid approximation where the effects of magnetic and electric fields on the flow are taken into account. A one-dimensional

treatment can not seamlessly simulate the entire interaction process from ISW collision with the bow shock to magnetopause displacement; consequently, this thesis will explore the ISW-bow shock interaction and magnetopause motion as two separate steps.

1.4 Research Objectives

This thesis has four objectives. The first objective is to develop an understanding of the physical processes associated with the displacement of the earth's bow shock and magnetopause initiated by collision of an ISW with the magnetosheath system. The second objective is to develop a one-dimensional numerical model of the ISW-magnetosheath interactions based upon gas-dynamic and MHD fluid equations that will allow determination of the displacements and velocities of the bow shock and the magnetopause. A third objective is to review and understand prior analytic treatments of the ISW-magnetosheath interactions, providing a basis for comparison with numerical results. And the fourth objective is to evaluate the performance of the numerical model by comparing simulation results with analytic solutions.

1.5 Thesis Overview

Following this introduction, Chapter II will provide a general background on plasma and shock physics. The background chapter begins by citing the March 24, 1991 Storm Sudden Commencement (SSC) event that resulted from an ISW impinging upon the earth's bow shock. A discussion of the near-earth environment is given after the SSC reference to establish the physical setting of the problem. Then, in the next section, some basic ideas about shock waves in ordinary gases and in plasmas are presented, along with

a discussion of the Rankine-Hugoniot relations that describe the conservation of mass momentum, and energy across a shock boundary. The discussion of shock waves is followed by a brief examination of the interactions of shock waves with other shock waves, and shock waves with regions of discontinuous jumps in density and temperature within a gas or plasma. Chapter II ends with a summary of the background material covered to that point.

Chapter III, a separate literature review, was deemed necessary to discuss in detail three articles that specifically examine the interaction of an interplanetary shock wave with the earth's magnetosheath system. The first article, by W. W. Shen and M. Dryer (1972), considers the interaction of an interplanetary shock wave with the bow shock; the second article, by Shen (1973) alone, describes the interaction of a shock wave with the magnetopause. The third article included in the literature review is a detailed work by S. A. Grib, et. al. (1979) which develops analytic solutions for shock wave-bow shock and shock wave-magnetopause interactions in both the gas-dynamic and MHD cases. The solutions developed by Grib provide a means to analytically determine position and velocity for the displaced bow shock and magnetopause as a function of the Mach number of the incident interplanetary shock wave; they also serve as a comparison to test how well the numerical simulation predicts bow shock and magnetopause motion.

Methodology is the subject of Chapter IV. The first section is a presentation of the design and development of a numerical model to simulate the ISW interaction with the earth's magnetosheath system. Development of the numerical model begins with the fluid conservation equations, from which a set of time and spatial dependent differential

4

equations for the conservation variables—i.e. mass density, momentum, magnetic field, and total energy—are derived. Next, the numerical algorithm for a one-dimensional, explicit, time dependent solution is discussed. This section also presents the procedure used to extract values for pressure, density, temperature, magnetic field, and flow velocity from updated conservation variables, as well as the method for determining shock front and contact discontinuity locations at each time step. After detailing the development of a numerical model, the next section examines the methodology of model validation.

Chapter V is a presentation of the simulation for four different ISW Mach numbers in both the gas-dynamic and the MHD cases. Here numerical solutions for bow shock and magnetopause position and velocity are given. Bow shock and magnetopause position and velocity determined from solutions to the analytic equations are also presented in this chapter, and the two sets of solutions are quantitatively compared.

Based on the results from Chapter V, the final chapter contains conclusions about model performance, its strengths and weaknesses, and its applicability to the problem of determining bow shock and magnetopause displacement due to an impinging ISW. Some comments are made concerning accomplishment of the research objectives and extension of this work beyond an investigation into separate bow shock and magnetopause movements to a continuous treatment of the entire magnetosheath displacement. And finally, at the end of this chapter, recommendations regarding model improvements and real-world validation are presented.

II. Background

At 03:41 UT on March 24, 1991 the formation of a new radiation belt near the equatorial plane at 2.55 earth radii was observed by the Combined Release and Radiation Effect Satellite (CRRES) at a point in its orbit which coincidentally passed through the inner edge of the formation region. This new radiation belt resulted from the interaction of an interplanetary shock wave which compressed the earth's magnetopause inside geostationary orbit and caused a surge in the geomagnetic field characteristic of a Storm Sudden Commencement (SSC) event (Li, 1993:2423). Magnetopause compression was accompanied by electron and ion drift echo events from which it was determined that energies of the electrons injected into this new radiation belt were greater than 15 MeV (Li, 1993:2423), and that the injected proton energies were in the range 20-80 MeV (Hudson, 1995:291). The radiation belt formed in less than 150 seconds and persisted beyond the end of the CRRES mission six months later (Li, 1993:2423). Xinlin Li successfully modeled the formation of the electron component of the new radiation belt resulting from the March 1991 SCC using a relativistic guiding center code (Li, 1993:2423); later M.K. Hudson used the same technique to model the proton component (Hudson, 1995:291).

The preceding example is cited to illustrate three ideas: that interplanetary shock waves, when they interact with the earth's magnetosphere, are capable of producing major changes in the near-earth environment; that compression, or motion, of the earth's

magnetopause is associated with changes in particle energies and distributions within the magnetosphere; and that it is possible to simulate these changes using a numerical computer model.

2.1 Space Environment

To understanding how interactions with interplanetary shock waves produce motions of the bow shock and magnetopause it is first necessary to understand the physical characteristics of the near-earth environment. Figure 1 is a representation of the near-earth environment.
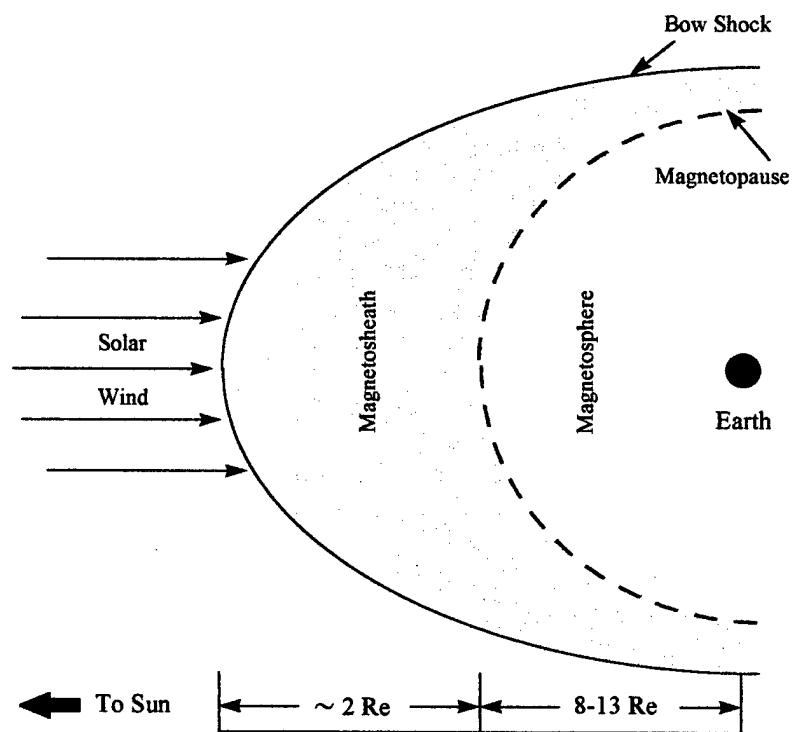
Figure 1. Earth bow shock-magnetopause system. Scale lengths are taken from Parks (1996:501-502).

Although it is commonly assumed that space is a vacuum, within the solar system there is in fact a tenuous gas made up almost entirely of ionized hydrogen atoms in the form of free protons and electrons streaming outward from the sun at velocities greater than the local speed of sound within the gas. This streaming ionized gas, or plasma, called the solar wind not only interacts with other matter kinetically as ordinary gases do, but its motion is also influenced by electric and magnetic fields in space. The properties of the solar wind vary, with values of flow speed, density, and magnetic field linked to changes on the sun's surface. Table 1 lists typical solar wind parameters, taken from Grib (1979:5909), that are used in numeric and analytic calculations later in this thesis.

Table 1. Solar Wind Parameters

Parameter	Value
Density , ρ_0 (kg/m^3)	1.837×10^{-20}
Temperature, T_0 (°K)	4.000×10^4
Flow Velocity, u_0 (km/sec)	280.0
Magnetic field, B_0 (Tesla)	3.500×10^{-9}
Pressure, P_0 (Pa)	0.121×10^{-10}
Sound Speed, a_0 (km/sec)	33.20
Thermal Velocity, V_{th} (km/sec)	18.18
Plasma Beta, β_0	2.490

As the solar wind flows toward the earth it encounters the magnetosphere, a region where the relatively strong magnetic field of the earth forms a protective cavity around which the solar wind is constrained to flow under the influence of electromagnetic forces. Upon encountering the magnetosphere, a bow shock wave forms in front of the magnetopause similar to the aerodynamic shock found in front of a blunt obstacle in supersonic wind tunnel experiments (Tascione, 1994:57). At the bow shock,

8

solar wind plasma undergoes rapid and dramatic increases in pressure, density, temperature, and magnetic field across the span of a few hundred kilometers; flow speed across the bow shock also changes from supersonic to subsonic flow (Grib:1979:5909). From data presented by Parks (1996:501), the bow shock appears to maintain a fairly consistent stand-off distance from the magnetopause of about two earth radii.

Between the bow shock and the magnetopause lies a region of compressed and heated solar wind plasma called the magnetosheath (Tascione, 1994:61). Here the magnetic field is more disordered than in the solar wind or in the magnetosphere, and the plasma is irregularly distributed through the region (Tascione, 1994:57).

The magnetopause is the boundary separating the interplanetary medium from the magnetosphere and is the surface where the outward force of the total magnetospheric pressure is balance by the force of the solar wind plasma pressure (Tascione, 1994:57). Total pressure, p*, is defined by Eq (1)

$$ p* = p + \frac{B^2}{2\mu_0} \qquad\qquad (1) $$

where,

   p = gas dynamic pressure,

and the second term on the right is magnetic pressure with,

   B = magnitude of the magnetic field,

   μ_0 = permeability of free space.

The magnetopause is classified as a tangential discontinuity (Parks,1996:335) meaning that, at the boundary, plasma flow velocity and magnetic field components normal to the surface are zero—they do not penetrate into the magnetosphere; density, temperature, and magnetic field, however, are allowed to change across the boundary to preserve the continuity of total pressures (Parks, 1996:329). Classifying the magnetopause as a tangential discontinuity requires that the solar wind decelerate through the magnetosheath so that, at the magnetopause, the velocity component normal to the surface satisfies the boundary condition—the point at which the velocity component becomes zero is called the stagnation point (Parks, 1996:317). The position of the magnetopause is very sensitive to changes in solar wind density, flow velocity, and to changes in strength and orientation of the Interplanetary Magnetic Field (IMF) (Tascione, 1996:57).

Inside the magnetopause lies the magnetosphere—the region of space immediately surrounding the earth permeated solely by the earth's magnetic field. It can be shown that the magnetic flux through a volume of solar wind plasma remains essentially unchanged, or "frozen-in", so that the IMF carried along by the solar wind does not penetrate into the magnetosphere as the flow is forced around the magnetopause. Satellite observations have shown that plasma density is lower, and temperature higher, just inside the magnetosphere than in the magnetosheath (Parks, 1996:338-39).

2.2 Shocks

A discussion of the earth's bow shock leads naturally to a closer examination of shock waves and shocks in space.

2.2.1 Sound Speed in Gases. In ordinary gases, collisions between gas particles transfer momentum and energy among the molecules, allowing compression acoustic waves to propagate through the medium. In an ideal gas, neglecting viscosity and heat conduction, and assuming an adiabatic compression, a disturbance will propagate through the gas at the speed of sound. Thus the speed of sound can be thought of as the speed at which information about a change in the state of a gas, or perturbation, is transmitted (Kivelson & Russell,1995: 130-131) and is given for an ideal isentropic gas by,

$$a = \sqrt{\frac{\gamma p}{\rho}} \qquad\qquad (2)$$

where,

a = speed of sound,

γ = isentropic exponent $\equiv$ ratio of specific heats C_p / C_v, = 5/3 for an ideal, monatomic gas,

p = gas pressure,

ρ = mass density.

2.2.2 Shock Formation. Shocks are formed by the steepening of compression waves in a gas. The speed of sound is the speed limit of an ordinary wave in a gas: a disturbance can not propagate through a gas faster than the sound speed unless the gas

11

changes from its original state in such a way that the sound speed increases. If the gas is described by the isentropic form of the equation of state, p/ρ^{γ} = constant (Wright, 1961:6); then for a disturbance resulting in a compression wave it can be shown that the new speed of sound, a_1, is

$$a_1 = a_0 \rho_1^{(\gamma-1)/2}$$ (3)

where,

a_0 = sound speed given by Eq (2) for p_0, ρ_0 in the undisturbed flow,

ρ_1 = higher density within the compression wave.

Density ρ_1 is greater within the compression wave than in the undisturbed gas; a_1 is therefore greater than a_0. Because the speed of sound is greatest at the peak of the compression wave where the density is highest, the peak of the wave will propagate faster and catch up to the front of the wave ahead of it, steepening the perturbation gradient of the wave until the flow becomes non-adiabatic, i.e. energy begins to flow into or out of the system so that changes become irreversible. At that point a balance is reached between steepening and dissipation due to viscosity and thermal conduction, resulting in a stable form of the wave front called a shock (Parks, 1996:416).

To illustrate the balance between steepening and dissipation, and their role in shock formation, an analytic solution to Burger's Equation is discussed. Burger's Equation describes the propagation of a perturbation wave in a non-linear fluid and is given by,

12

$$\frac{\partial p(x,t)}{\partial t} - c\frac{\partial p(x,t)}{\partial x} - \alpha\, p(x,t)\frac{\partial p(x,t)}{\partial x} = ac^3\frac{\partial p(x,t)}{\partial x} \qquad (4)$$

where,

p(x, t) = a perturbation in a fluid as a function of position, x, and time, t;

c = propagation speed of the wave;

α = coefficient of the non-linear term $p(x,t)\dfrac{\partial p(x,t)}{\partial x}$;

a = wave dampening coefficient (Landau, 1959:351).

Transforming to a wave-centered reference frame moving along with the wave at speed c, Eq (4) becomes,

$$\frac{\partial p'(\xi,t)}{\partial t} + p'(\xi,t)\frac{\partial p'(\xi,t)}{\partial \xi} = \mu\frac{\partial p'(\xi,t)}{\partial \xi} \qquad (5)$$

here,

p′(ξ, t) = - α p (x, t)

ξ = characteristic of the wave propagation, in this case a wave moving to the

right given by x + c t,

μ = dissipation term, a c^3.

The solution to the transformed Burger's Equation (Eq (5)), p′ (ξ, t), is derived using the

techniques of Vvedensky (1992:274-79,361-66) and has the form,

$$p'(\xi,t) = \left(\cfrac{2(\mu/\alpha)}{\cfrac{1}{e^{(\alpha/2\mu)}-1} + \cfrac{1}{2}\mathrm{erfc}\left(\cfrac{\xi-x_0}{\sqrt{4\mu t}}\right)} \right) \cfrac{1}{\sqrt{4\pi\mu t}} \, e^{\left(\frac{-(\xi-x_0)^2}{4\mu t}\right)} \qquad (6)$$

where,

x_0 = the initial position of the perturbation at time $t_0 = 0$,

erfc = the complimentary error function.

Figure 2 illustrates wave steepening and broadening by showing plots of p $(\xi,\, t)$ at three different times.
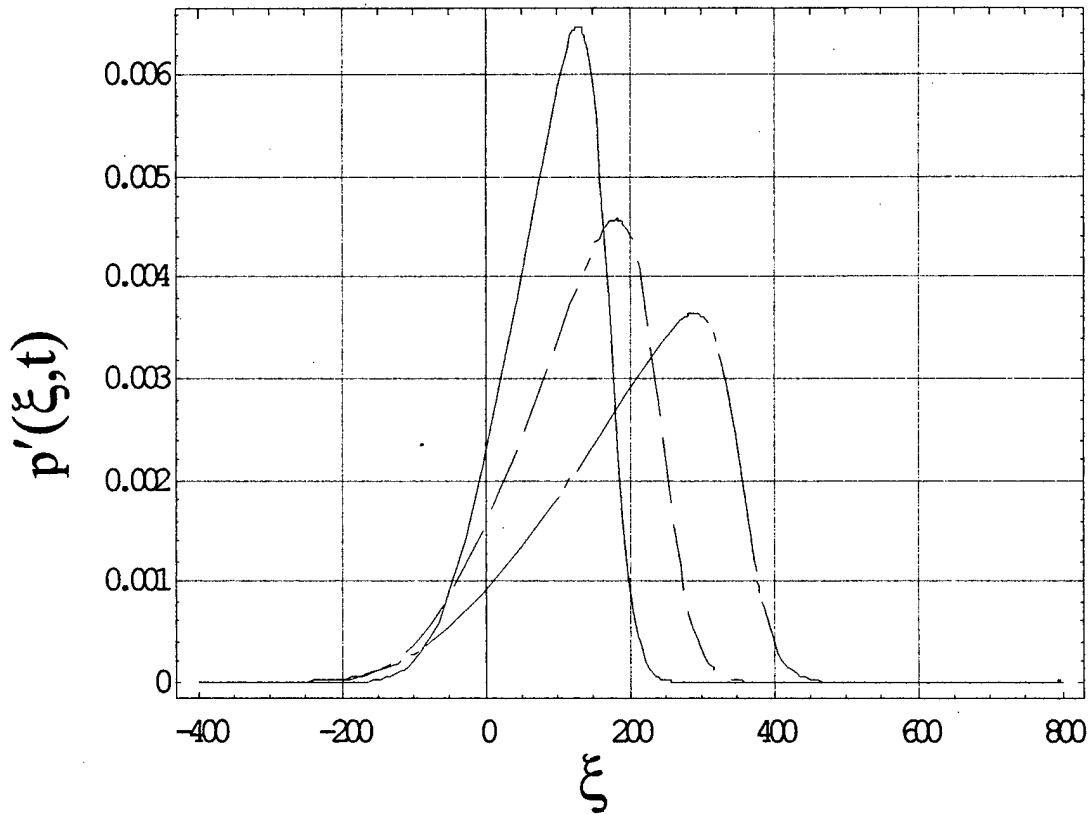
Figure 2. Wave Front Steepening

14

From Eq (6) steepening and broadening of the wave front depend on the values

of α and μ: a larger coefficient of non-linearity causes the wave to steepen faster in time

and to have a steeper slope; greater dissipation causes the wave to steepen more slowly

and to have a more inclined slope. When non-linear and dissipative terms in Eq (5) are

equal, then $\partial p(\xi, t)/\partial t = 0$ and a steady wave form is achieved.

The same effects of wave steepening manifest by Eq (6) are observed when a

disturbance propagates through a gas at supersonic speeds. At speeds greater than the

sound speed non-linear effects proportional to the velocity become important so that a

wave front steepens, and when dissipation within the gas balances steepening, a steady

shock wave is formed For purposes of this thesis a shock is defined as a disturbance

propagating at supersonic speed through a plasma as a steady wave front that irreversibly

alters the state of the gas behind it. (Kivelson & Russell, 1995:131)

2.2.3 Shocks in Space. Shocks in space, however, are more complicated

because interplanetary plasmas are more rarefied than ordinary gases and the presence of

electric and magnetic fields in space affect plasma wave propagation. According to

Kivelson and Russell (1995:129), "Collisions in an ordinary gas serve to transfer

momentum and energy among the molecules, and they provide the coupling that allows

the basic wave, the sound wave, to exist." Plasmas in space are so tenuous that

collisional coupling is essentially absent (Kivelson and Russell, 1995:129). Parks

(1996:414) indicates that the exact mechanisms for shock formation in space plasmas are

not yet identified but suggests that plasma collective effects and wave-particle

interactions may play a part in the processes. If in the macroscopic regime the following

15

assumptions are made: that the charged plasma particles behave as a single entity and that Coulomb forces between them are negligible, the plasma is in thermal equilibrium, and the motion of the plasma is affected by electric and magnetic fields; then the plasma behaves as an ideal fluid--this is the Magnetohydrodynamic (MHD) approximation (Parks, 1996:141). Plasmas behaving as ideal fluids in the MHD approximation are governed by the same relationships that allow shock waves to form in ordinary gases; the difference is that in the MHD case there are four different types of waves, three of which are compressional and can lead to shock formation in space.

2.2.4. **Magnetosonic Shocks**. The four types of waves possible in a magnetized plasma are the acoustic wave, the Alfvén wave, and the fast and slow magnetosonic waves—of these four, only the Alfvén wave is not compressional. For propagation perpendicular to the magnetic field, the Alfvén and slow magnetosonic waves vanish (Parks, 1996:418) so that only acoustic and fast magnetosonic waves are available to form shocks. Just like the acoustic wave, the fast magnetosonic wave has a propagation speed, called the fast magnetosonic sound speed, which depends on the characteristics of the plasma through which it travels. The fast magnetosonic sound speed, c_f, is given by

$$c_f = \sqrt{a^2 + V_A{}^2} \qquad\qquad (7)$$

where,

a = sound speed (Eq (1)),

$V_A \equiv$ Alfvén wave speed $= (B^2/\mu_0\, \rho)^{1/2}$,

B = magnetic field.

16

Similar to an acoustic wave, if a magnetosonic wave propagates through a magnetized plasma at a speed greater than c_f, then it, too, will steepen to become a fast magnetosonic shock. The fast magnetosonic speed of magnetospheric plasma is a key parameter in determining magnetopause motion.

2.2.5 Rankine-Hugoniot Relations. As discussed in Section 2.2.2, shock waves are non-adiabatic regions where kinetic energy of the fluid is converted to thermal energy through dissipation; the total energy of the fluid, however, must remain the same. Conversion between forms of energy at a shock necessitates changes in plasma parameters. Figure 3 is representative of changes, or jumps, in plasma parameters across a generic shock located at the mid-point of each panel; numbers in each panel indicate unshocked, 0, and shocked, 1, plasma.
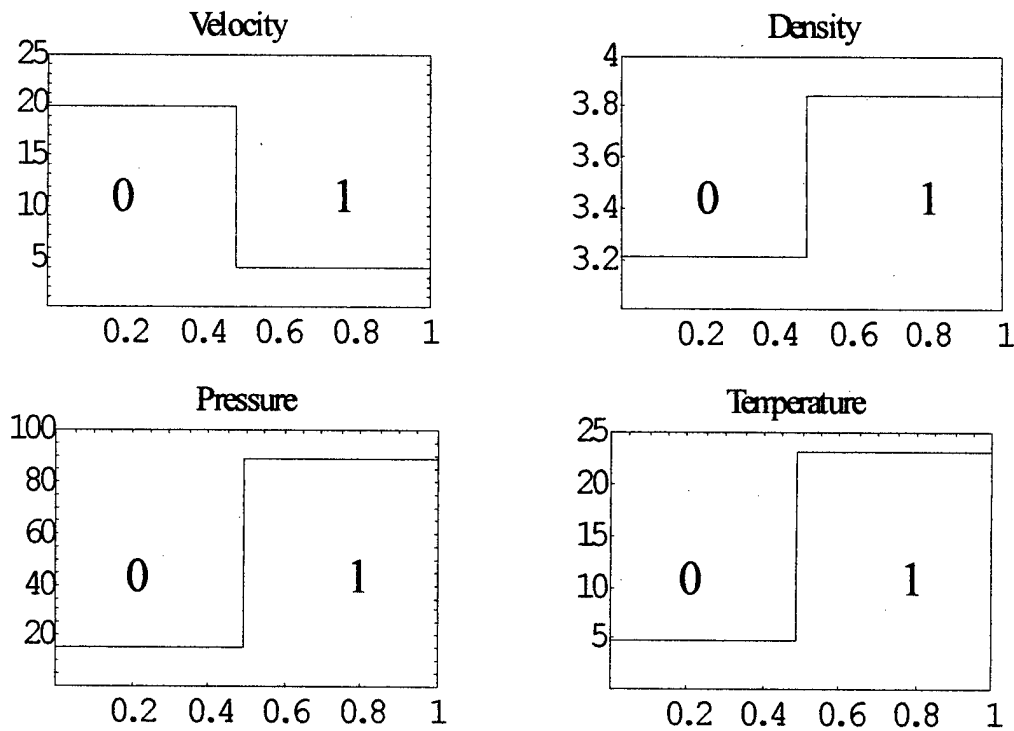
Figure 3. Shock jump conditions

Conservation of mass, momentum, and energy across a shock require the following relations to be true:

$$[\rho u] = 0 \qquad (8)$$

$$[\rho u^2 + p] = 0 \qquad (9)$$

$$\left[\left(\frac{\rho u^2}{2} + \frac{\gamma p}{(\gamma - 1)}\right) u\right] = 0 \qquad (10)$$

where, u = gas flow velocity (Parks, 1996:421). The bracket notation indicates the difference between the included quantities on the two sides of a shock; e.g., $[\rho u] = 0$ means $\rho_1 u_1 - \rho_0 u_0 = 0$, where the subscripts 1, and 0 correspond to the shocked, and unshocked regions of Figure 3. Equations (8) - (10) are the Rankine-Hugoniot relations in the gas-dynamic case and from them the ratios of density, pressure, flow velocity, and temperature between the two sides of a shock are determined. These ratios, or jump conditions, are valid in the shock-centered reference frame and are given by,

$$\frac{\rho_1}{\rho_0} = \frac{(\gamma + 1)M^2}{(\gamma - 1)M^2 + 2} = \eta \qquad (11)$$

$$\frac{p_1}{p_0} = \frac{2\gamma M^2 - (\gamma - 1)}{(\gamma + 1)} = y \qquad (12)$$

$$\frac{u_1}{u_0} = \frac{(\gamma - 1)M^2 + 2}{(\gamma + 1)M^2} = \eta^{-1} \qquad (13)$$

$$\frac{T_1}{T_0} = \frac{y}{\eta} \qquad (14)$$

18

where,

$M \equiv$ Mach number = ratio of the shock propagation speed, V, relative to the

upstream speed of sound = V/a_0,

$\eta \equiv$ shock compression ratio, or compressibility,

$y \equiv$ shock strength (Parks, 1991:422).

The Rankine-Hugoniot relations for the MHD case, From Grib (1979:5908), are:

$$\left[\rho u\right] = 0 \tag{15}$$

$$\left[B u\right] = 0 \tag{16}$$

$$\left[\rho u^2 + p + \frac{B^2}{2\mu_0}\right] = 0 \tag{17}$$

$$\left[\frac{\rho u^2}{2} + \frac{\gamma p}{(\gamma-1)} + \frac{B^2}{\mu_0}\right] = 0 \tag{18}$$

From Equations (15) - (18) the MHD jump conditions are found:

$$\zeta = \frac{\mu}{2} + \frac{1+1/\beta_0}{(\gamma+1)M^2} + \sqrt{\left(\frac{\mu}{2} + \frac{1+1/\beta_0}{(\gamma+1)M^2}\right)^2 + \left(\frac{2(2-\gamma)}{\gamma(\gamma+1)\beta_0 M^2}\right)} \tag{19}$$

$$\zeta^{-1} = \frac{\rho_1}{\rho_0} = \frac{B_1}{B_0} \tag{20}$$

$$\frac{p_1}{p_0} = 1 + \gamma M^2(1-\zeta) - \frac{1}{\beta_0}\left(\frac{1}{\zeta^2} - 1\right) \tag{21}$$

$$\frac{u_1}{u_0} = \zeta \tag{22}$$

$$\frac{T_1}{T_0} = y\zeta \qquad\qquad (23)$$

where,

$\zeta \equiv$ degree of compressibility $= \eta^{-1}$ (Eq (13)),

$\beta_0 =$ plasma beta of the upstream gas $\equiv 2 \mu_0 p_0/B_0^2$,

$\mu = (\gamma-1)/(\gamma+1)$ (Grib, 1979:5908). Here again, subscripts refer to the shocked and unshocked regions of Figure 3. When the magnetic field is zero β goes to infinity and the MHD jump conditions reduce to the gas-dynamic jump conditions. From Eq (20) the magnetic field ratio is equal to ζ^{-1}, meaning that B varies as density across a shock. Using the jump conditions, plasma parameters on either side of a shock can be found if the shock Mach number and the parameters on the other side are known.

2.3 Shock Interactions

After discussing the near-earth environment and shocks, the final piece of background information presented is an examination of interactions between shocks, discontinuities, and rafefaction waves—waves in which the density and pressure decrease, while the magnitude of the velocity increases. An incoming interplanetary shock wave (ISW) is a shock wave propagating through the ambient solar toward the earth. As it approaches earth, the ISW interacts with the bow shock—a shock-shock interaction—generating two new shock waves that move inward toward the earth at different speeds. The slower shock wave in effect becomes the new bow shock; the faster shock wave rapidly traverses the magnetosheath to interact with the magnetopause—a shock-discontinuity interaction. The interaction of the fast shock wave

with the magnetopause creates a third new shock wave transmitted into the magnetosphere and a new contact discontinuity that becomes a new magnetopause also moving toward the earth. Shock-shock and shock-discontinuity interactions will be examined separately in the next two sections.

2.3.1 Shock-Shock Interactions. According to Landau and Lifshitz, when two shock waves intersect the result will be two new shock waves separated by a contact discontinuity (1959:408-409). A contact discontinuity is a surface characterized by jumps in density and temperature from one side to the other, but across which plasma velocity and pressure are continuous. The following continuity relationships therefore apply across a contact discontinuity:

$$[u] = 0 \qquad\qquad (24)$$

$$[\rho] \neq 0 \qquad\qquad (25)$$

$$\left[p + \frac{B^2}{2\mu_0} \right] = 0 \qquad\qquad (26)$$

Courant and Friedrichs (1948:179) reached a similar conclusion when they determined that collisions between two shocks of different strengths produces two new shock waves moving away from each other in a reference frame moving with the contact discontinuity.

Figure 4 depicts a shock-shock interaction representing the ISW-bow shock collision on an x-t (distance-time) diagram. In this figure the ISW and bow shock

21

intersect at time t_1 resulting in two new shocks, S_3 and S_4, with a contact discontinuity, C_1, between them consistent with Landau and Lifshitz.
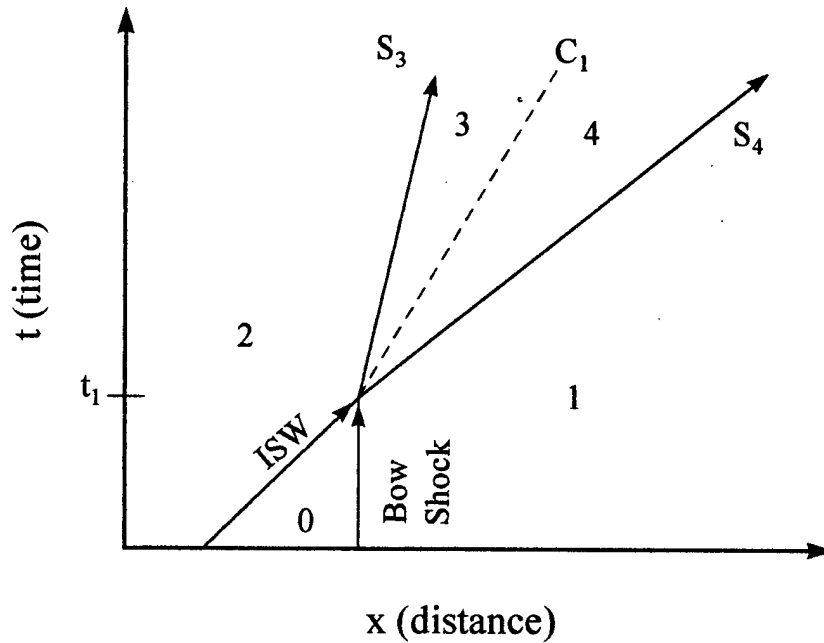
Figure 4. x-t diagram for shock-shock interaction

The propagation speed of a shock is determined from an x-t diagram by the inverse of the slope drawn through its x, t coordinates; faster shocks have a slope that is more horizontal while a vertical line represents a stationary feature. The reference to Courant and Friedrichs would seem to indicate that C_1 in Figure 4 should be drawn as a vertical line with S_3 and S_4 propagating in opposite directions; that all three structures are shown traveling to the right in the positive x direction is an illustration that they propagate along with the bulk plasma flow toward the earth.

The numbers in Figure 4 correspond to regions of plasma "shocked", or altered by one or more of the depicted shock waves. By convention, in a reference frame traveling with a shock wave, unshocked plasma flowing into the shock is designated as the "upstream" plasma, while "shocked" plasma flowing out is referred to as the "downstream" plasma. Region 0 refers to the pre-interaction, unshocked, ambient solar wind, while Region 1 represents plasma from Region 0 shocked by the stationary bow shock. In a similar manner Region 2 depicts upstream solar wind plasma shocked by an advancing ISW. After t_1, the upstream plasma shown flowing into S_3 comes from Region 2, and Region 1 plasma becomes the upstream flow into S_4; 3 and 4 therefore depict regions of twice-shocked plasma.

2.3.2 Shock-Discontinuity Interactions. Turning again to Landau and Lifshitz, (1959:408) the collision between a shock wave and a tangential discontinuity produces a reflected rarefaction wave, a new shock wave, and a contact discontinuity. Courant and Friedrichs (1948:179) establish that if the second medium has a lower sound speed, or if the incident shock is sufficiently weak, then a rarefaction-shock wave pair is produced when a shock impinges on a contact discontinuity. Figure 5 is an x-t depiction of the interaction between the shock wave generated by the ISW-bow shock intersection, S4, and the magnetopause represented as a tangential discontinuity.
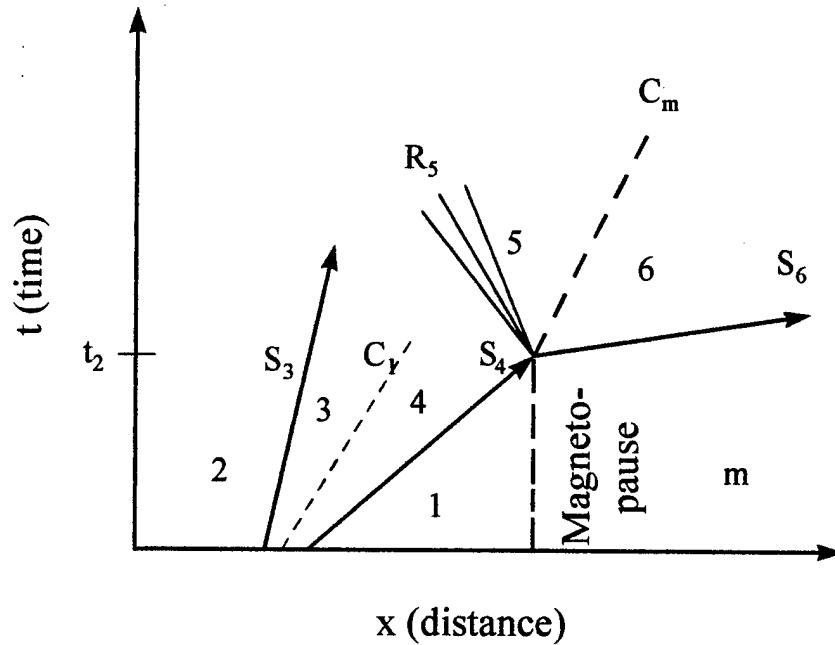
Figure 5. S_4 - magnetopause interaction

Here, the time is extended so that S_4 collides with the magnetopause at t_2 to produce a

shock transmitted into the magnetosphere, S_6, a reflected rarefaction wave, R_5, and a

contact discontinuity between them, C_m, representing the new magnetopause moving

toward the earth. Regions 1, 2, 3, and 4 are the same as in Figure 4. Regions 5 and 6 are

the regions downstream from R_5, S_6, and Region m is the undisturbed magnetosphere.

The slope of S_6 was drawn at a more horizontal angle to the x-axis to illustrate

that, upon crossing into a region of lower density and higher temperature, the propagation

speed of a shock wave increases Wright (1961:79). A second point regarding Figure 5 is

that, although R_5 is depicted propagating to the left, this may not be necessarily true. A

rarefaction wave is not a shock and thus propagates at the local speed of sound within the

24

plasma. If the sound speed is less than the flow speed of the plasma in Region 4, then R_5 will propagate along with the plasma flow to the right (Grib, 1979:5911).

2.4 Background Summary

Before moving on to the next chapter a brief summary of the background material may be helpful. The author can only handle simple ideas, so this summary will attempt to distill the important points into nut-shell concepts that the reader can take with him through the remainder of this thesis.

Three broad topics were touched upon: the near-earth environment, shocks in plasmas, and interactions between shocks. The near-earth environment is "filled" with a very thin plasma flowing supersonically toward the earth from the sun. The formation of shock waves in space plasmas are more difficult to understand, but if a few simplifying assumptions about how plasma particles interact with each other and with electomagnetic fields, then to a good approximation the plasma behaves as an ideal gas. Shocks are boundaries across which plasma parameters change rapidly. Fortunately a set of simple mathematical relationships exist which allow plasma parameters on one side of a shock or discontinuity to be determined if parameters on the other side are known. And finally, in the case of an interplanetary shock wave impinging on the magnetosheath system, bow shock and magnetopause displacement is determined by shock-shock and shock-discontinuity interactions. The sequence of events is as follows: first, an ISW impinges upon the stationary bow shock creating two new shock waves: a fast shock which quickly traverses the magnetosheath to interact with the magnetopause, and a slower shock that becomes the new bow shock moving in towards the earth; and then, at the magnetopause,

the fast shock wave collides, resulting is a third shock wave transmitted into the

magnetosphere, a rarefaction wave propagating back toward the advancing bow shock (if

the plasma flow speed in the disturbed magnetosheath is less than the speed of sound),

and a new magnetopause also moving in toward the earth.

III. <u>Literature Review</u>

A review of the pertinent literature yielded three articles directly treating the subject of the bow shock and magnetopause motion induced through collision with an interplanetary shock wave. The first article, by Shen and Dryer (1972), discusses the interaction of an interplanetary shock wave with the earth's bow shock and provides a technique to solve for the propagation speeds of the resulting shock waves. The second article, by Shen (1973) alone, is a qualitative study of the interaction of a shock wave with the magnetopause. The third article is a detailed work by Grib, et. al. (1979) which develops analytic solutions for shock-bow shock and shock-magnetopause interactions in both the gas-dynamic and MHD cases. Grib's solutions provide a means to analytically determine position and velocity for the displaced bow shock and magnetopause as a function of the Mach number of the incident interplanetary shock wave; they can also serve as a validation tool to asses the ability of the numerical model developed in this thesis to predict bow shock and magnetopause motion.

3.1 Shen and Dryer

Shen and Dryer (1972) formulated the interaction as a one dimensional problem in which the interplanetary shock, a fast magnetosonic wave propagating through the solar wind from the sun to the earth, collides with a standing bow shock (1972:4628-29). Echoing earlier treatments by Courant and Friedrichs, and Landau and Lifshitz, Shen and Dryer discuss the formation of two new shock waves, S_3 and S_4, with a contact discontinuity, C_1, between them generated by the ISW-bow shock interaction. Applying

continuity of flow velocity and pressure (Equations (24) and (26), with B = 0) across C_1

for the gas-dynamic case, they obtain the following equations:

$$\frac{\left[2\gamma M_4{}^2 - (\gamma - 1)\right]\left[2\gamma M_1{}^2 - (\gamma - 1)\right]}{\left[2\gamma M_3{}^2 - (\gamma - 1)\right]\left[2\gamma M_2{}^2 - (\gamma - 1)\right]} = 0 \qquad (27)$$

and,

$$\frac{1 - M_2{}^2}{M_2(\gamma + 1)} - G(M_2, \gamma)\left[\frac{1 - M_3{}^2}{M_3(\gamma + 1)}\right] - \frac{1 - M_1{}^2}{M_1(\gamma + 1)} - G(M_1, \gamma)\left[\frac{1 - M_4{}^2}{M_4(\gamma + 1)}\right] = 0 \quad (28)$$

where,

$$G(M, \gamma) = \left\{\left[\frac{2\gamma M^2 - (\gamma - 1)}{\gamma + 1}\right]\left[\frac{2 + M^2(\gamma - 1)}{(\gamma + 1)M^2}\right]\right\}^{1/2}$$

is the square root of the ratio of the shock strength and compressibility, $\sqrt{(y/\eta)}$, for

specified Mach number, M, and isentropic exponent, γ (Shen, 1972:4631). Simultaneous

solutions of Equations (27) and (28) yield the Mach numbers, M_3 and M_4, of the two

generated shocks in terms of the known bow shock and ISW Mach numbers, M_1 and M_2.

To more realistically describe the ISW-bow shock interaction, Shen and Dryer

include magnetic effects by applying the MHD form of Equations (24) and (26) (B ≠ 0);

continuity of flow velocity and total pressure across C_1 are then expressed as,

$$\begin{aligned} A_1\beta(M_1, A_1) + A_4\beta(M_4, A_4)\left[\xi(M_1, A_1)\right]^{1/2} \\ - A_2\beta(M_2, A_2) + A_3\beta(M_3, A_3)\left[\xi(M_2, A_2)\right]^{1/2} = 0 \end{aligned} \qquad (29)$$

and,

$$\frac{\delta(M_1,A_1)\delta(M_4,A_4)}{2M_0^2} + \frac{\xi^2(M_1,A_1)\xi^2(M_4,A_4)}{2A_1^2}$$

$$-\frac{\delta(M_2,a_2)\delta(M_4,A_4)}{2M_1^2} + \frac{\xi^2(M_1,A_1)\xi^2(M_4,A_4)}{2A_1^2} = 0 \qquad (30)$$

where,

$A \equiv$ Alfvén number $=$ the ratio of the wave speed, V, to the

Alfvén speed, V_A,

$$\beta(M,A) = \frac{A^2 + M^2 - A^2 M^2}{3A^2 M^2},$$

$$\xi(M,A) = \frac{3A^2 M^2}{2M^2 + 2A^2 + M^2 A^2},$$

with A_3 and A_4 given by,

$$A_3 = \frac{M_1}{A_1} \frac{\left[\delta(M_3,A_3)\right]^{1/2}}{\xi(M_3,A_3)} \qquad (31)$$

$$A_4 = \frac{M_1}{A_1} \frac{\left[\delta(M_4,A_4)\right]^{1/2}}{\xi(M_4,A_4)}. \qquad (32)$$

Shen and Dryer define $\xi(M,A)$ as the MHD compressibility and $\delta(M,A)$ as the MHD

shock strength (Shen, 1972:4633). The simultaneous solutions of Equations (29) - (32)

yield acoustic Mach numbers M_3 and M_4, and the Alfvén numbers, A_3 and A_4, for shock

waves S_3 and S_4.

With the Mach and Alfvén numbers of the generated shocks determined, then relationships given by Shen and Dryer in Table 2 can be used to determine the propagation speeds of S_3 and S_4 through the magnetosheath.

Table 2. Mach number relations for shock-bow shock interaction

Shock	Acoustic Mach Number	Alfvén Number	Magnetosonic Mach Number
S_1	$M_1 = (u_0\text{-}V_1)/a_0$	$A_1 = (u_0\text{-}V_1)/b_0$	$M^*_1 = (u_0\text{-}V_1)/c_0$
S_2	$M_I = (u_0\text{-}V_2)/a_0$	$A_2 = (u_0\text{-}V_2)/b_0$	$M^*_2 = (u_0\text{-}V_I)/c_0$
S_3	$M_3 = (u_2\text{-}V_3)/a_2$	$A_3 = (u_2\text{-}V_3)/b_2$	$M^*_3 = (u_2\text{-}V_R)/c_2$
S_4	$M_4 = (u_1\text{-}V_4)/a_1$	$A_4 = (u_1\text{-}V_4)/b_1$	$M^*_4 = (u_1\text{-}V_4)/c_1$

from: Shen and Dryer (1972:4633)

where the form is $M_k = (u_i - V_k)/a_i$, and,

u_i = gas flow velocity in Region i of Figure 4, $i = 0, 1, 2$,

V_k = shock propagation speed of the kth shock, $k = 1, 2, 3, 4$,

a_i = speed of sound Eq (1) in Region i,

b_i = Alfvén speed in Region i,

c_i = fast magnetosonic sound speed c_f Eq (7) in Region i.

These relationships hold in the absolute, or earth-centered, reference frame. Note that the absolute frame is also the bow shock reference frame because V_1, the propagation speed of the bow shock before collision with the ISW, is taken to be equal to zero.

3.2 Shen

In his second paper, Shen (1973) considers the interaction of S_4 with a stationary magnetopause characterized as a tangential discontinuity (1973:55). He again proceeds along the same lines as Courant and Friedrichs, and Landau and Lifshitz, by qualitatively

30

describing the formation of a new shock wave, S_6, and a reflected rarefaction wave, R_5, resulting from the S_4-magnetopause collision (see Figure 5). Invoking the continuity of plasma flow velocity and pressure across the new contact discontinuity, C_m, also formed in this collision, Shen states that a system of four equations in four unknowns can be solved to yield the Alfvén number for R_5 and the Mach number for S_6; he does not, however provide the equations to complete the solution. He does provide a useful table of relationships for the Alfvénic and acoustic Mach numbers presented in Table 3.

Table 3. Mach number relations for shock-magnetopause interaction

Shock	Ordinary Mach Number	Alfvén Number	Magnetosonic Mach Number
S_4	$M_4 = (V_4 - u_1)/a_1$	$A_4 = (V_4 - u_1)/b_1$	$M^*_1 = (V_4 - u_1)/c_1$
R_5	$M_5 = (V_5 - u_4)/a_4$	$A_5 = (V_5 - u_4)/b_4$	$M^*_5 = (V_5 - u_4)/c_4$
S_6	$M_6 = (V_6 - u_m)/a_m$	$A_6 = (V_6 - u_m)/b_m$	$M^*_6 = (V_6 - u_m)/c_m$

from Shen (1973:54)

where the subscripts now refer to the regions in Figure 6, and,

u_i = gas flow velocity in Region i of Figure 6, i = 1, 4, and m,

V_k = wave propagation speed of kth wave, k = 4, 5, and 6.

Two additional points discussed by Shen deserve mention here. The first is that observations indicate density "is sharply cut off at the boundary of the magnetospheric cavity" (1973:56), further supporting that the case of interest when S_4 interacts with the magnetopause is the generation of a reflected rarefaction wave (recall Courant and Friedrichs). The second point is that because of lower density and a small plasma β inside the magnetosphere, the propagation speed of S_6 inside the magnetosphere is substantially higher than the velocity of the shock wave S_4 (1973:59).

31

3.3 Grib

The third and final paper reviewed is an excellent treatise by S. A. Grib, et. al.,
(1979) on the entire problem from the ISW collision with the bow shock to
magnetopause retrograde motion toward its initial position. This paper is mathematically
rich and most of the equations derived therein are important to the development of this
thesis; therefore many of their equations will be included in this review for reference in
the next chapter. To ensure that proper credit is given to other's work and yet avoid
repeated reference to the same source, subsequent citations within this chapter from Grib,
et. al. (1979) will reference only the page number unless otherwise stated.

As Shen and Dryer before them, Grib, et. al. assume a one-dimensional problem.
They also state that only the component of the magnetic field perpendicular to the flow
velocity—i.e. in the z direction—is significant to the problem (5908), thus the fast
magnetosonic and acoustic waves are the only waves of concern. As preparatory
material they also give two useful equations, based on the Riemann invariants, for plasma
flow speed behind a rarefaction wave in the gas-dynamic (Eq (33)) and MHD (Eq (34))
cases:

$$ u \mp \frac{2}{\gamma - 1} a = \mp \frac{2}{\gamma - 1} a_0 = \text{const} \qquad (33) $$

$$ u \pm \frac{2}{\gamma - 1} a J_e(\alpha) = \pm \frac{2}{\gamma - 1} a_0 J_e(\alpha) \qquad (34) $$

where the subscript 0 refers to upstream, "unshocked" values, and

$\quad$ u $\equiv$ gas flow speed,

$\alpha = V_A{}^2 / a^2 = B^2 / 2\mu_0\rho a^2 \equiv$ the ratio of Alfvén speed to sound speed,

$$J_e(\alpha) \equiv \int_0^1 \sqrt{1 + \alpha x^{2\gamma/\gamma-1}}\, dx.$$

Proceeding along the same lines as Shen and Dryer, Grib describes the creation of the two new shocks, S_3 and S_4, and the contact discontinuity between them, resulting from the ISW-bow shock collision as illustrated in Figure 4. Given a Mach number for the ISW and ambient solar wind conditions, then the flow parameters for plasmas in Region 1 and Region 2 are easily determined from the shock jump equations. Assuming that the bow shock is stationary in the earth reference frame determines that the upstream flow velocity into the bow shock is just the ambient solar wind speed; Region 1 values are constant for a given ambient solar wind and do not change until disturbed by passage of S_4. Parameters behind the incoming ISW depend on the Mach number M_2 and on the conditions of the upstream solar wind, but for any given solar wind conditions parameters in Region 2 depend only on M_2.

Applying equality of pressure and velocity across the contact discontinuity, and assuming that u_2, p_2, u_1, and p_1 are known variables, Grib arrives at a system of two equations in M_3 and M_4 (for the gas-dynamic case):

$$u_2 - \frac{2a_2}{\gamma - 1}\frac{M_3{}^2 - 1}{M_3} = u_1 + \frac{2a_1}{\gamma - 1}\frac{M_4{}^2 - 1}{M_4} \tag{35}$$

$$p_2\left(\frac{2\gamma}{\gamma + 1}M_3{}^2 - \frac{\gamma - 1}{\gamma + 1}\right) = p_1\left(\frac{2\gamma}{\gamma + 1}M_4{}^2 - \frac{\gamma - 1}{\gamma + 1}\right). \tag{36}$$

33

Here, the left hand sides of Equations (35) and (36) are the flow speed and pressure in

Region 3; the right hand sides are the flow speed and pressure in Region 4. Solving these

equations simultaneously result in solutions of M_3 and M_4 in terms of M_2. Grib also

defines the Mach number of the plasma flow in Region 2 as $M^* = u_2 / a_2$. The numerical

solutions of Equations (35) and (36).are plotted in Figure 6, for Mach Numbers M_3, M_4,

and M^* in terms of M_2 for the gas-dynamic case. '
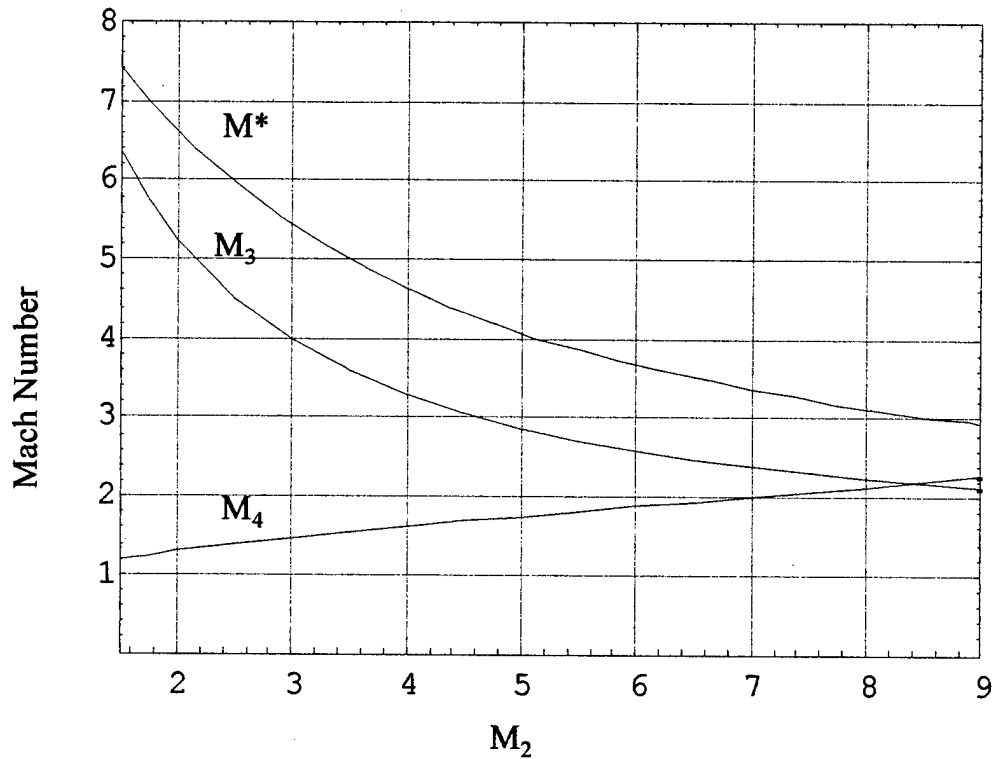
Figure 6. Mach numbers for gas-dynamic ISW-bow shock interaction.
M3 is the Mach number for the reflected shock, M4 is the Mach number
of the transmitted shock, and M* is the Mach number of the fluid flow
downstream of the ISW.

Knowing M_4 and a_1, Grib develops an equation to determine the time, $t_2 - t_1$,

required for S_4 to cross the magnetosheath and reach the magnetopause. In the earth-

centered reference frame, the new bow shock, S_3, travels toward the earth with a velocity

$a_2(M^* - M_3)$ (5909); until S_4 reaches the magnetopause at time t_2, the thickness of the magnetosheath decreases as S_3 moves earthward. Defining the initial thickness of the magnetosheath as δ, then the change in thickness at some $\Delta t = t_2 - t_1$ is

$$\left| \delta_1 - \delta \right| = \int_0^{\Delta t} a_2(M^* - M_3)\,dt \qquad (37)$$

where,

δ_1 is the new magnetosheath thickness,

and Δt, the time it takes S_4 to traverse the magnetosheath, given by,

$$\Delta t = \int_0^{\delta_1} \frac{dx}{\left(u_1(1-\delta/x)+a_1M_4\right)} = \frac{\delta}{u_1}\ln\left(1+\frac{u_1}{a_1M_4}\right) \approx \frac{\delta}{a_1M_4}. \qquad (38)$$

(5910)

Eq (38) is based on the assumption that the flow velocity in the undisturbed magnetosheath reduces linearly to zero at the magnetopause. Eq (37) allows the position of the moving bow shock to be determined as the change in magnetosheath thickness in a time Δt.

Having determined the Mach numbers M_3 and M_4, and, consequently, all of the plasma parameters in Regions 3 and 4 by application of the jump conditions, Grib turns to a solution of the S_4-magnetopause interaction. Before S_4 arrives at the magnetopause, there must be a balance of pressures between the magnetosheath and the magnetosphere—a boundary condition for a tangential discontinuity (recall Parks, 1991:329). However, observations show that density inside the magnetosphere is

35

significantly lower than in the magnetosheath so that, from the ideal gas law, pressure in the magnetosphere, p_m, is much lower than p_1 and the gas dynamic approach fails. Because dynamic pressure alone in the magnetopause is insufficient to balance the pressure from the magnetosheath, Grib adopts a quasi-gas-dynamic approach in which the dynamic pressure of the solar wind is balanced by the sum of dynamic and magnetic pressures within the magnetosphere. By including the magnetic pressure of the earth's relatively strong planetary field, pressure balance is achieved across the magnetopause even though p_m is less than p_1 (5911).

Collision of S_4 with the magnetopause produces a new shock, S_6, transmitted into the magnetopause, a reflected rarefaction wave, R_5, propagating sunward toward the incoming bow shock, and a new contact discontinuity, C_m, which in effect becomes the new magnetopause moving with the flow velocity in Region 5 and 6 toward the earth (see Figure 5). The rarefaction wave is not a shock and therefore propagates as an acoustic wave (5908) into Region 4. In the absolute reference frame the rarefaction wave travels at velocity $a_4 - u_4$ so that R_5 will travel toward the advancing bow shock only if $a_4 > u_4$. For solar wind parameters listed in Table 1, $a_4 > u_4$ if $M_2 \leq 5$ (5911). It will be shown at the end of this chapter that the interaction of rarefaction waves is a mechanism that reverses the earthward motion of the bow shock and magnetopause. Thus, when $M_2 > 5$, the rarefaction wave can not propagate sunward to interact with the advancing bow shock and eventually reverse its.

At the new magnetopause, C_m, continuity of total pressure and flow velocity, and the Riemann invariants associated with the rarefaction wave (Eq (33)) results in a set of

36

two equations in terms of ρ_5, the density in Region 5, and M_6, the Mach number of the shock wave propagated into the magnetosphere:

$$u_4 + \frac{2}{\gamma - 1}(a_4 - a_5) = (1 - \zeta)a_6 M_6 \qquad (39)$$

and,

$$p_1 \left[\frac{2\gamma M_4^2 + 1 - \gamma}{\gamma + 1} \right] \left[\frac{\rho_5}{\rho_1} \right]^\gamma \left[\frac{(\gamma - 1)M_4^2 + 2}{(\gamma + 1)M_4} \right]^\gamma = p_m \left(1 + \frac{1 - \zeta}{1 + 1/\beta} \gamma M_6^2 \right) \qquad (40)$$

where $\zeta = \zeta (M_6, \beta_m)$ (Eq (19)), and,

$$a_5 = a_4 \left(\frac{\rho_5}{\rho_4} \right)^{(\gamma - 1)/2} \qquad (41)$$

$$p_5 = p_4 \left(\frac{\rho_5}{\rho_4} \right)^\gamma . \qquad (42)$$

$$(5911)$$

Knowing the Mach number of an approaching interplanetary shock wave, M_2, and the conditions of the solar wind, Equations (35), (36), and (39) - (42) permit analytic gas-dynamic solutions for M_3, M_4, and M_6 in terms of M_2. These Mach numbers are then used to determine bow shock and magnetopause motions, as well as plasma parameters in each region of Figures 4 and 5.

Just as Shen and Dryer before them, Grib, et. al. repeat their analysis for the MHD case by including the effects of magnetic fields on shock wave propagation in a plasma. Here the full MHD forms of the Rankine-Hugoniot equations and shock jump equations must be used. The physical arguments leading to the formation of two new shocks upon

collision of the ISW with the bow shock, and the rarefaction wave-transmitted shock pair resulting from the S_4-magnetopause interaction, do not change in the MHD approach so that Figures 4 and 5 still represent these interactions. Different forms of the compressibility, ζ, and the shock strength, y, lead to different jump equations and to different relationships for pressure and velocity continuity across a contact discontinuity. Grib expresses the relationships for continuity of pressure and velocity at the contact discontinuity C_1 as

$$u_2 - a_2 M_3 (1 - \zeta_3) = u_1 + a_1 M_4 (1 - \zeta_4) \qquad (43)$$

$$p_2^* \left(1 + \frac{1 - \zeta_3}{1 + 1/\beta_2} \gamma M_3{}^2 \right) = p_1^* \left(1 + \frac{1 - \zeta_4}{1 + 1/\beta_1} \gamma M_4{}^2 \right) \qquad (44)$$

where,

$p^* \equiv$ the total pressure (Eq (1)),

$\zeta \equiv$ compressibility ratio in terms of the Mach number M and β *upstream* of the shock (Eq (19)),

$\beta \equiv$ the ratio of magnetic to dynamic pressure $= B^2/(2 \mu_0 p)$ (5913).

Similar to the gas-dynamic treatment, Equations (43) and (44) are solved simultaneously to obtain M_3 and M_4 for the MHD case and the results are presented in Figure 7.
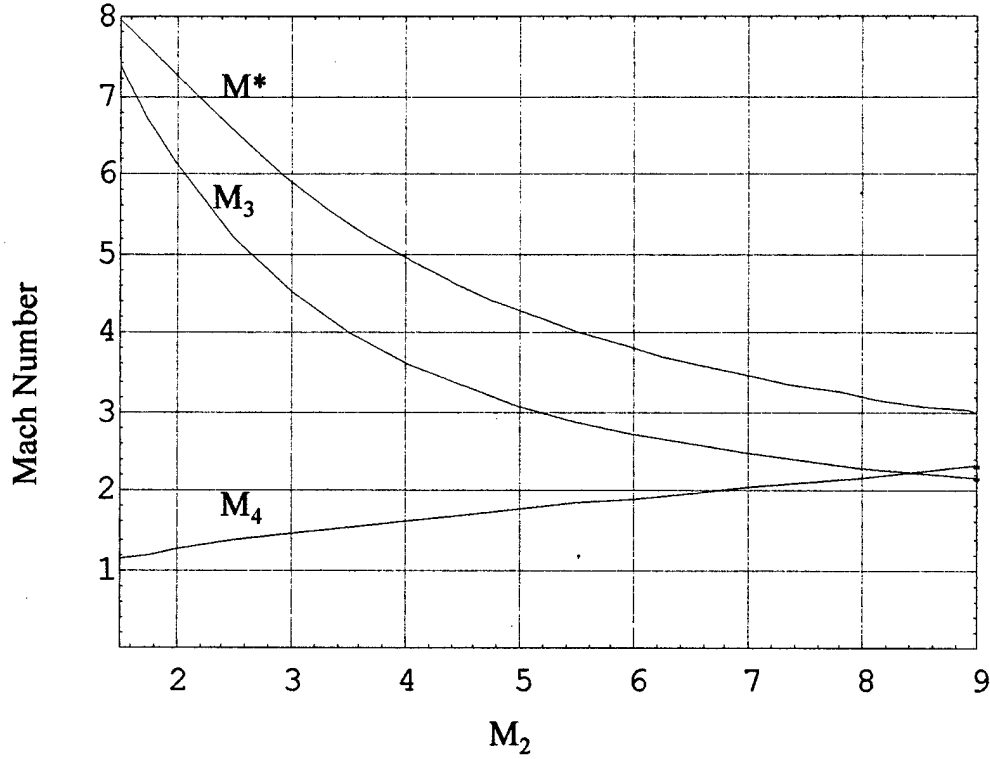
Figure 7. Mach numbers for MHD ISW-bow shock interaction.

The solution for M_4 and the plasma conditions behind the shock S_4, allow Grib to make the next step in the analysis: an examination of the flow velocities and total pressures in Regions 5 and 6 that will enable a solution for M_6 and the plasma parameters behind the transmitted shock. At the new magnetopause, C_m, equality of flow speed is given by

$$(1-\zeta_4)a_1 M_4 + \frac{2}{\gamma-1}\left[a_4 J_e(\alpha_4) - a_5 J_e(\alpha_5)\right] = (1-\zeta_6)a_6 M_6 \qquad (45)$$

where,

$$\alpha_5 = \frac{B_1^{\,2}}{\mu_0\, p_4 \zeta_4}\left(\frac{\rho_5}{\rho_1}\right)^{2-\gamma}$$

$$a_5{}^2 = a_4{}^2 \left(\frac{\rho_5 \zeta_4}{\rho}\right)^{\frac{\gamma-1}{}}$$

and, continuity of pressure gives,

$$p_4 \zeta_4 \left(\frac{\rho_5}{\rho_1}\right)^\gamma + \frac{B_1{}^\gamma}{2\mu_0}\left(\frac{\rho_5}{\rho_1}\right)^2 = p_m \left(1+\frac{1-\zeta_6}{1+1/\beta_m}\gamma M_6\right). \qquad (46)$$

Solving Equations (45) and (46) simultaneously results in a determination of the two unknowns, ρ_5 and M_6. Equations (43) - (46) form a set of simple analytical relationships from which the MHD Mach numbers for all three generated shocks are found in terms of M_2. With these Mach numbers, along with the ambient conditions in the solar wind and magnetopause, plasma parameters in each region of Figures 4 and 5 are determined for the MHD case. The new magnetopause will move with the flow at speed u_6 after collision with S_4; the new bow shock, S_3, moves with a speed $u_2 - (1 + M_3)a_2$ (Grib,5913).

Having determined the conditions of the magnetosheath up to a time just after the creation of S_6 and the rarefaction wave R_5, Grib et. al. take their examination one step farther by determining when and how the magnetopause will reverse its earthward movement. They describe a series of successive rarefaction waves reflecting off of the advancing bow shock rear and the magnetopause as depicted in Figure 8. The first rarefaction wave, R_5, decreases the particle density and pressure in the magnetosheath as it travels against the flow toward the bow shock. It will reach the bow shock only if its speed is greater than the flow velocity in the magnetosheath, requiring $M_2 \geq 6$ for $B_0 = 3.5 \times 10^{-9}$ Teslas (nT) (:5915). At the rear of the bow shock, a new rarefaction wave, or

rarefaction fan, labeled R_8 reflects off of the bow shock and moves toward the

magnetopause; the bow shock speed increases slightly as it advances into the region of

lower density caused by R_5. Traversing the magnetosheath, R_8 encounters the

magnetopause where it decreases the flow pressure just behind C_m, allowing the

magnetopause to slow and to reverse direction moving back against the flow. The

reversed magnetopause now "pushes" on the gas in front of it much like a piston in a

shock tube, creating multiple small perturbations in pressure that steepen into a new

shock which interacts with the bow shock to produce a new bow shock S_{10} (:5914-15).
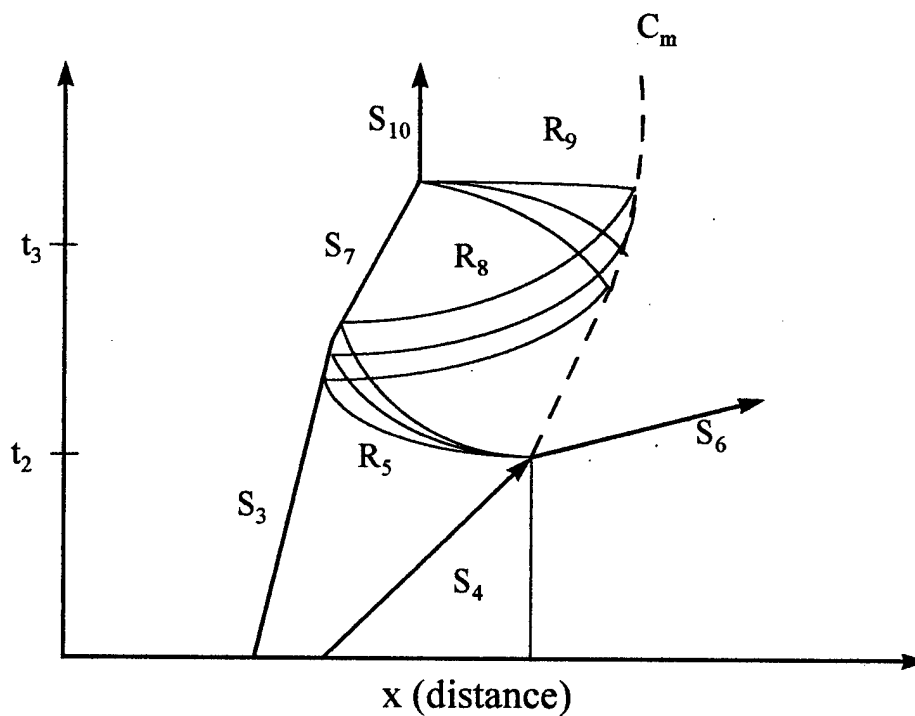
Figure 8. Rarefaction wave interactions (Grib, 1979:5911)

In their paper, Grib and his colleagues arrive at an equation of magnetopause

motion in the form,

$$x = (u_6 - c_6)t + (c_6 + c_5)t\left(\frac{\tau}{t}\right)^{c_5/(c_5+c_6)} - c_5\tau \qquad (47)$$

where,

$\tau \equiv$ time between arrival of the shock S_4 and the arrival of $R_8 = t_3 - t_2$,

$c =$ fast magnetosonic speed in Regions 5 and 6, respectively (:5915).

Consistent with Grib's explanation of magnetopause reversal, Figure 8 is drawn to depict the magnetopause turning to coincide with the intersection of R_8 which occurs at time τ after the initial shock impact. Grib, et. al. provide estimated limits for τ based upon the magnetic field of the solar wind, B_0. For $B_0 = 0$ $\tau = 1$-3 minutes; for $B_0 = 3.5$ nT $\tau = 3$-5 minutes; and for $B_0 = 7.0$ nT $\tau = 7$ minutes (Grib, 1979:5914).

3.4 Literature Review Summary

In this literature review three articles were discussed: Shen and Dryer's treatment of the ISW-bow shock interaction, Shen's paper on the S_4-magnetopause interaction, and the detailed analysis of the complete ISW-magnetosheath interaction presented by Grib, et. al. From Shen and Dryer comes a technique for solving sets of gas-dynamic and MHD equations for the unknown Mach numbers of the shock waves generated by the ISW-magnetosheath interaction; i.e. application of the continuity of plasma flow velocity and pressures across a contact discontinuity and simultaneous solution of the resulting equations for the Mach numbers. Shen's second paper is a qualitative discussion of the shock-discontinuity interaction. In the article by Grib, et. al., the technique of Shen and Dryer is applied to both the ISW-bow shock and the S4-magnetopause interactions to

yield sets of gas-dynamic and MHD equations which are then solved to determine the unknown Mach numbers of the generated shock waves. Applying the Mach number solutions to the shock jump equations allows plasma parameters in each region of the modified magnetosheath to also be determined, leading to solutions for bow shock and magnetopause motion. Extending their treatment beyond the initial motions of the bow shock and magnetopause, Grib, et. al. arrive at an equation of magnetopause motion which describes the reversal of the magnetopause movement resulting from the repeated interaction of rarefaction waves between the bow shock and magnetopause.

IV. <u>Methodology</u>

The earlier works of Shen , Dryer, and Grib lay a qualitative and analytic foundation toward understanding bow shock and magnetopause displacement resulting from collision with an interplanetary shock wave. To advance the understanding of the physical processes associated with bow shock and magnetopause motion, and to approximate to a reasonable degree of confidence the displacements and velocities resulting from these processes, a one-dimensional numerical model is developed to simulate the ISW-magnetosheath interactions. This chapter is a presentation of the development, validation, and execution of this numerical model.

Development of the numerical model begins with the fluid conservation equations, from which a set of time and spatially dependent differential equations for the conservation variables—i.e. mass density, momentum, magnetic field, and total energy— are derived. Next, the numerical algorithm used for a one-dimensional, explicit, time dependent solution of the differential equations is discussed. Procedures used to extract pressure, density, temperature, magnetic field, and flow velocity from conservation variables updated by the model, as well as the method for determining shock front and contact discontinuity locations at each time step are also presented.

After detailing the development of the numerical model, the next discussion examines the procedures used to validate the numerical model. To verify that the algorithm generates reasonable and expected results, several test cases are executed and

the results are analyzed and compared to shock propagation speeds derived from known analytic solutions.

The final section in Chapter IV describes model input, initialization procedures, and data processing.

4.1 Model Development

There are several advantages of adopting a numerical approach to determine bow shock and magnetopause displacement when analytic solutions already exist. One advantage is that a numerical simulation allows observation of the time evolution of the shock-shock and shock-discontinuity interactions. Another advantage is that a numerical simulation quickly provides a reasonable approximation of not only bow shock and magnetopause displacement, but it also yields information about plasma conditions—i.e. pressure, density, temperature, magnetic field, and flow velocity—for each region of the interacting system at each time step. As a consequence of this ability to determine plasma parameters in different regions, a numerical simulation can simultaneously track the progression of several different shock waves, contact discontinuities, and rarefaction waves. A third advantage is that the complicated interactions between rarefaction waves and the bow shock and magnetopause described by Grib, et. al. can theoretically be simulated by numerical code. To arrive at their equation of magnetopause motion (Eq (47)), Grib and his colleagues made evaluations of rarefaction wave propagation based on average velocities of the waves through different plasma regions (Grib, 1979:5912, 5914); by tracking changes in plasma parameters characteristic of a rarefaction wave, numerical simulations would provide better estimates of rarefaction wave position and

velocity.

4.1.1. Equation Development. Development of a numerical model began with the vector MHD fluid equations given by Tóth (1996:83) reduced to the one dimensional case:

$$\frac{\partial \rho}{\partial t} + \frac{\partial}{\partial x}(\rho u) = 0 \qquad (48)$$

$$\frac{\partial}{\partial t}(B) + \frac{\partial}{\partial x}(uB) = 0 \qquad (49)$$

$$\frac{\partial}{\partial t}(\rho u) + \frac{\partial}{\partial x}(\rho uu) = -\frac{\partial}{\partial x}(p^*) \qquad (50)$$

$$\frac{\partial}{\partial t}(e) + \frac{\partial}{\partial x}(eu) = -\frac{\partial}{\partial x}(up^*) \qquad (51)$$

where,

e = total energy density = $\dfrac{\rho u^2}{2} + \dfrac{p}{(\gamma - 1)} + \dfrac{B^2}{2\mu_0}$,

p^* = total pressure (Eq (1)).

Substituting e and p^* into the fluid equations, Equations (48) - (51) become,

$$\frac{\partial \rho}{\partial t} + \frac{\partial}{\partial x}(\rho u) = 0 \qquad (52)$$

$$\frac{\partial}{\partial t}(B) + \frac{\partial}{\partial x}(uB) = 0 \qquad (53)$$

$$\frac{\partial}{\partial t}(\rho u) + \frac{\partial}{\partial x}\left(\rho u^2 + p + \frac{B^2}{2\mu_0}\right) = 0 \qquad (54)$$

$$\frac{\partial}{\partial t}\left(\frac{\rho u^2}{2}+\frac{p}{\gamma-1}+\frac{B^2}{2\mu_0}\right)+\frac{\partial}{\partial x}\left(u\left\{\frac{\rho u^2}{2}+\frac{\gamma p}{\gamma-1}+\frac{B^2}{\mu_0}\right\}\right)=0. \tag{55}$$

Equations (52) - (55) form a set of time and spatially dependent partial differential equations in the conservation variables. This set of equations can be written in a convenient matrix form,

$$\frac{\partial Q}{\partial t}+\frac{\partial F}{\partial x}=0 \tag{56}$$

where,

$$Q=\begin{pmatrix}\rho \\ B \\ \rho u \\ \dfrac{\rho u^2}{2}+\dfrac{p}{\gamma-1}+\dfrac{B^2}{2\mu_0}\end{pmatrix} \tag{57}$$

and,

$$F=\begin{pmatrix}\rho u \\ Bu \\ \rho u^2+p+\dfrac{B^2}{2\mu_0} \\ u\left\{\dfrac{\rho u^2}{2}+\dfrac{\gamma p}{\gamma-1}+\dfrac{B^2}{\mu_0}\right\}\end{pmatrix}. \tag{58}$$

It is often desirable to non-dimensionalize a set of equations used in a numerical model to simplify calculations. Equations (57) - (58) are non-dimensionalized by applying the parameter transformations listed below:

47

$$x' = \frac{x}{L} \qquad\qquad t' = t\frac{V_{th}}{L}$$

$$u' = \frac{u}{V_{th}} \qquad\qquad p' = \frac{p}{p_0}$$

$$\rho' = \frac{\rho}{\rho_0} \qquad\qquad T' = \frac{T}{T_0}$$

$$B' = \frac{B}{B_0}$$

where,

L = scale length of the model,

V_{th} = thermal velocity of the solar wind = $(k\ T_0/m)^{1/2}$, and the superscript 0 refers to the ambient solar wind values of the indicated parameters. The non-dimensionalized Q and F matrices are,

$$Q = \begin{pmatrix} \rho' \\ B' \\ \rho'u' \\ \dfrac{\rho'u'^2}{2} + \dfrac{2p'}{\gamma-1} + \dfrac{2B'^2}{\beta_0} \end{pmatrix} \qquad\qquad (59)$$

and,

$$F = \begin{pmatrix} \rho'u' \\ B'u' \\ \rho'u'^2 + 2p' + \dfrac{2B'^2}{\beta_0} \\ u'\left(\dfrac{\rho'u'^2}{2} + \dfrac{2\gamma p'}{\gamma-1} + \dfrac{2B'^2}{\beta_0} \right) \end{pmatrix} \qquad\qquad (60)$$

48

where the primed notation signifies dimensionless parameters and β_0 is defined as the ratio of magnetic to dynamic pressure, $B_0^2 / (2\, \mu_0\, p_0)$, in the solar wind. Note that the factor 2 multiplying pressure and magnetic field terms in Equations (59) and (60) is due to an ideal gas law in the form $p = 2\, n\, k\, T$ which accounts for a quasi-neutral plasma in which the number densities and temperatures of ions and electrons are assumed equal. The ideal gas law becomes $p \approx 2\, \rho\, k\, T/m$, where ρ is the ion mass density and m is the ion mass, when the mass of the ions are much greater than the mass of the electrons.

The function of the algorithm is to numerically update Q in time. To determine shock and discontinuity locations, however, plasma pressure, density, temperature, magnetic field, and flow velocity must be known at each bin in the model at successive time steps. These quantities are calculated from values of Q by the following equations:

$$\rho' = Q(1) \tag{61}$$

$$B' = Q(2) \tag{62}$$

$$u' = \frac{Q(3)}{Q(1)} \tag{63}$$

$$p' = \left[Q(4) - \frac{1}{2} Q(1) Q(3)^2 - \frac{2}{\beta_0} Q(2)^2 \right] \left(\frac{\gamma - 1}{2} \right) \tag{64}$$

$$T' = \frac{p'}{Q(1)}. \tag{65}$$

The numbers in parentheses refer to elements of the Q matrix.

Equations (48) - (65) are valid for both the gas-dynamic and MHD fluid approximations. If, in these equations B = 0, then magnetic terms drop out and the gas-dynamic equations is recovered.

4.1.2. Algorithm Development. With the derivation of the governing fluid equations complete, the next step was the development of a suitable numeric algorithm to advance solutions of the equations in time. The core algorithm selected was a MacCormack predictor-corrector scheme with Flux Corrected Transport (FCT) taken from Fletcher's book, <u>Computational Techniques for Fluid Dynamics: Vol II, Techniques for Different Flow Categories</u> (1991:154-156). This finite difference technique is effective in capturing shock locations within a steady inviscid supersonic flow (1991:147); it is also fairly computationally simple and can be implemented on a desktop computer. FCT is a technique incorporated into the algorithm to reduce numerical oscillations at locations where steep gradients, such as shock waves and discontinuities, cause numerical instabilities. The technique adds higher order diffusive terms to broaden a shock or discontinuity over a greater number of spatial bins, thus decreasing the gradient and the associated instabilities. Higher order anti-diffusive terms are then subtracted out of the diffused solution to recover a physically meaningful result. The art in the technique is to add diffusive terms and subtract anti-diffusive terms in just the right amounts (Tóth, 1996:82).

The MacCormack algorithm solves the conservation equations of mass, magnetic flux, momentum, and energy in the form,

$$\frac{\partial Q}{\partial t} + \frac{\partial F}{\partial x} = 0 \qquad (56)$$

across each bin advancing Q in time by two stages (Fletcher, 1991:148). Here Q and F are the matrices derived in Equations (59) and (60). The first, or predictor stage, obtains an intermediate solution

$$Q_j^* = Q_j^n - \frac{\Delta t}{\Delta x}\left(F_{j+1}^n - F_j^n\right) \qquad (66)$$

which is then put into the second, or corrector stage

$$Q_j^{n+1} = 0.5(Q_j^n + Q_j^*) - \frac{\Delta t}{2\Delta x}\left(F_j^* - F_{j-1}^*\right) \qquad (67)$$

where,

superscript n designates the value at time $t_n = \sum_i n \Delta t_i$,

subscript j is the spatial bin index,

Δx = spatial bin width in dimensionless units,

Δt = optimized, dimensionless time step for time t_n,

Q^* is the intermediate solution of the predictor stage,

F^* is the intermediate value of F as a function of Q^*. (Fletcher, 1991:149).

The time step, Δt, must be constrained to ensure that gas flow does not advance more than one bin in a single step, otherwise the model may become unstable. The desired time step is one in which $[| u_j |]_{max} \Delta t \le \Delta x$, where $[| u_j |]_{max}$ is the absolute value of the speed taken from the bin with the largest flow velocity. To guarantee that flow advances at most only one bin in a time step, the right hand side of the inequality is multiplied by a factor less than one called the Courant-Friedrich-Levy (CFL) factor (Tóth,

1996:84), which in the present code is a constant equal to 0.25. From Tóth, (1996:84), the time required to step the model so that changes in mass, momentum, and energy fluxes propagate no more than one bin is,

$$\Delta t \leq CFL \frac{\Delta x}{\left[\left| u_i \right| + c_{q,i}\right]_{max}} \ . \tag{68}$$

The denominator in Eq (68) is the wave propagation speed in the absolute reference frame taken from the bin having the largest absolute value of $\left| u_i \right| + c_{q,i}$. Here c_q, the speed of the fast mode MHD wave, is

$$c_q = \frac{1}{\sqrt{2}}\left[\frac{\gamma p + B^2}{\rho} + \sqrt{\left(\frac{\gamma p + B^2}{\rho}\right)^2 - 4\frac{\gamma p B^2}{\rho^2}}\right]^{1/2} \tag{69}$$

(Tóth, 1996:84).

In dimensionless form Eq (69) becomes,

$$c'_q = \left[\gamma T' + \frac{B'^2}{\beta_0 \rho'} + \sqrt{\left(\gamma T' + \frac{B'^2}{\beta_0 \rho'}\right)^2 - 4\frac{\gamma T' B'^2}{\rho'}}\right]^{1/2} \ . \tag{70}$$

Equations (69) - (70) are valid for both the gas-dynamic and MHD cases. If B = 0, then magnetic terms drop out and c_q becomes just the acoustic wave speed.

Following stages one and two, Q is sent to the FCT subroutine where a diffusive flux, DF, is added to reduce the gradients in parameter jumps, (Eq (68))

$$Q_j = Q_j + DF_j - DF_{j-1} \tag{71}$$

and anti-diffusive fluxes, ADFs, are subtracted (Eq (69)) to recover the desired solution.

$$Q_j = Q_j + ADF_{j-1} - ADF_j \qquad (72)$$

The details of how DF and ADF are calculated provided in Fletcher's book.

The last step in the MacCormack algorithm is to extract from Q^{n+1} the new gas parameters in each bin, which is accomplished using Equations (61) - (65) derived in Section 4.1.1.

An enhancement to the basic code was the inclusion of a new procedure to locate multiple structures—shocks and discontinuities—from the data extracted from Q^{n+1}. A density jump, or large density gradient, is a feature common to both shock waves and discontinuities and is relatively easy to extract from algorithm data. A new subroutine was written to locate bins where the density gradient, $\Delta\rho/\Delta x$, exceeded a threshold value of 100, corresponding to a density change of approximately four percent between adjacent bins. The routine begins at the largest bin number and progresses sequentially backward (from right to left) testing density gradients at each bin. When the gradient exceeds the threshold value, the routine enters a second loop, beginning at the current bin, and continues testing backwards until the gradient again drops below the threshold criteria—thus the location of a structure is bracketed between right and left bins. With the structure now bracketed, the subroutine selects the mid-point as the location of the structure and stores the location for further processing back in the main program. After determining the location of a structure, the subroutine returns to the main counter loop and continues working backwards until another qualifying density gradient triggers the bracketing routine. At each time step, the main program compares the previous location

53

of each structure to the location returned by the subroutine. If a structure's location has changed, the program updates the previous location and writes the new location to a data file. This procedure can track up to eight shocks and discontinuities.

4.1.3. Model Adaptation. The MacCormack algorithm is typically employed to find numerical solutions to the Riemann, or shock tube problem. In a Riemann problem, gases in a cylinder are separated into two isolated regions by a thin, non-permeable membrane and maintained at different pressures, densities, and temperatures as shown in

Figure 9(a). The shock tube experiment begins when the membrane is ruptured suddenly and the two gases, initially at rest, are allowed to freely flow. The usual result is the formation of a shock wave propagating from the region of higher pressure into the lower pressure region, and an expansion of lower pressure in the opposite direction as depicted in Figure 9 (b).
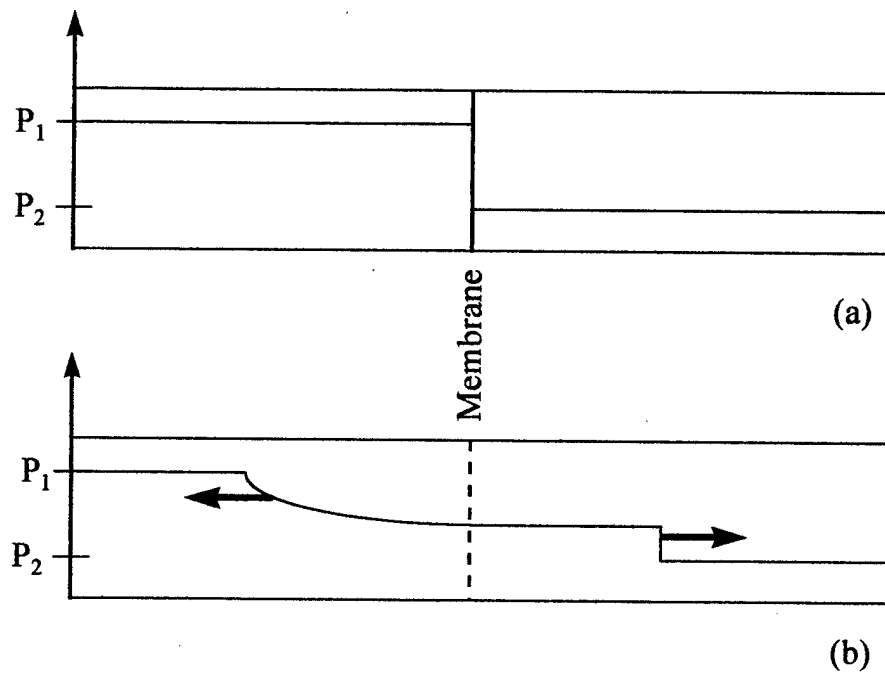
Figure 9. Shock tube problem.

Unlike the shock tube problem, plasmas in the solar wind and the magnetosheath are seldom at rest. To realistically simulate the magnetosheath system and the interactions resulting from collision with the bow shock, the boundary conditions must be adapted to permit a steady flow into, and out of, the model. The problem of simulating a stationary bow shock at the boundary between the solar wind and the magnetosheath requires a steady supersonic solar wind flow into the shock.

Tascione compared the bow shock to the aerodynamic stand-off shock that forms in front of a blunt obstacle in supersonic wind tunnel experiments (1994:57); in fact, data from Parks suggests that the bow shock maintains a fairly constant stand-off distance from the magnetopause of about two earth radii (1996:501-502). Figure 10 is a

representation of the earth's stationary bow shock characterized by a jump from solar wind pressure, p_0, to magnetosheath pressure, p_1.
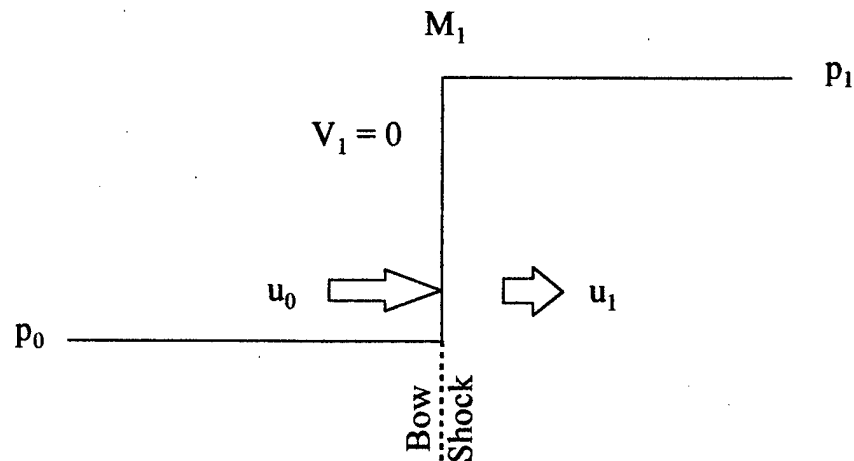
Figure 10. The bow shock

The bow shock will move or remain stationary depending on what reference frame is chosen. In Figure 10 two velocities are depicted on the left side of the bow shock—the solar wind flow speed, u_0, and the bow shock propagation speed, $V_1 = 0$, in the absolute—or earth-centered—reference frame. Transforming to the rest frame of the solar wind, $u_0 = 0$, and the bow shock would move to the left with a shock speed $V_1 = M_1 a_0 = -u_0$, where M_1 is the bow shock Mach number determined by the upstream solar wind sound speed and the flow speed into the shock. The case in which $u_0 = 0$ and the bow shock propagates to the left is a classic Riemann problem of a shock wave

propagating into a plasma at rest. Observations indicate that the bow shock is relatively

stationary, i.e. $V_1 = 0$, in the absolute reference frame, requiring that the solar wind flow

supersonically into the shock, and sub-sonically behind the shock at the magnetopause

flow velocity u_1, in order to maintain its structure and location. Thus, in order to

maintain a stationary shock in a flowing plasma, the model was adapted to incorporate

steady plasma flow into and out of the boundaries.

A deficiency in the algorithm was the inability to simulate a stationary shock

wave in a flowing plasma. It was found that a stationary shock would develop a

temperature trough, or a sharp decrease in temperatures within a few bins immediately

upstream of a shock front. See Figure 11.
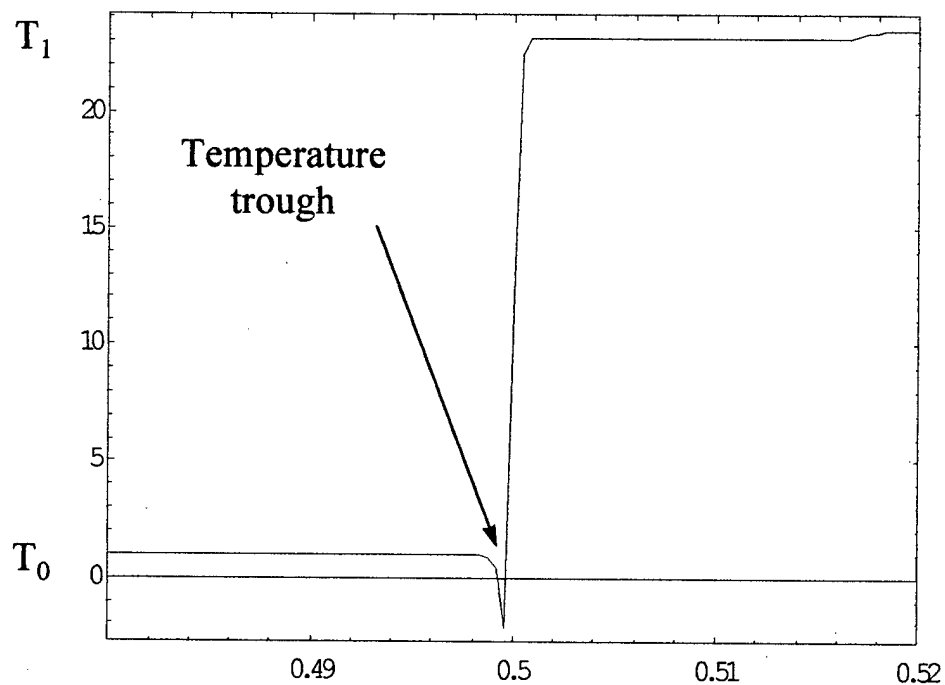
Figure 11. Temperature trough.

Formation of a temperature trough seemed to occur only for stationary shock waves which, in the fluid reference frame, propagate against plasma flow (see Figure 10). The magnitude of the drop in temperature at the shock front also seemed to have a dependence on the magnitude of the stationary shock, which is determined by the speed of the upstream plasma flowing into the shock. Temperature drops appeared greater for higher Mach numbers: in fact, formation of a temperature trough was not observed until an attempt was made to simulate a stationary Mach 5 shock. Although too few simulations were made to draw any definite conclusions, it is believed that formation of temperature troughs may be a result of numerical instabilities in the code arising from shock waves propagating against the flow of a plasma. Figure 11 was produced from data generated by the MacCormack algorithm attempting to model a stationary bow shock in a plasma characterized by the solar wind parameters found in Table 1, and a flow velocity of 280 km/sec. The Mach number of the bow shock, M_1, was determined to be 8.44 from the definition of Mach number, $M = V/a_0$, based on a shock propagation speed of -280 km/sec and a solar wind sound speed of 33 km/sec.

The purpose of FCT is to reduce numerical oscillations resulting from steep parameter gradients in a finite-difference approximation algorithm. It was found that multiplying the DF terms in the FCT subroutine by a factor of 1.5; corrected temperature trough formation associated with a stationary shock front. Figure 12 shows the effect of multiplying the diffusive terms of the FCT subroutine by a DF coefficient of 1.5, all other variables and inputs to the algorithm were exactly the same as in the model run that produced Figure 11. The simulation yielded a shock front that remained unchanged from

58

the one depicted in Figure 12 through 500 iterations of the algorithm. Adjusting the

amount of diffusive flux added to the raw numerical solution resulted in a steady,

stationary simulation of the bow shock in a supersonic plasma flow.
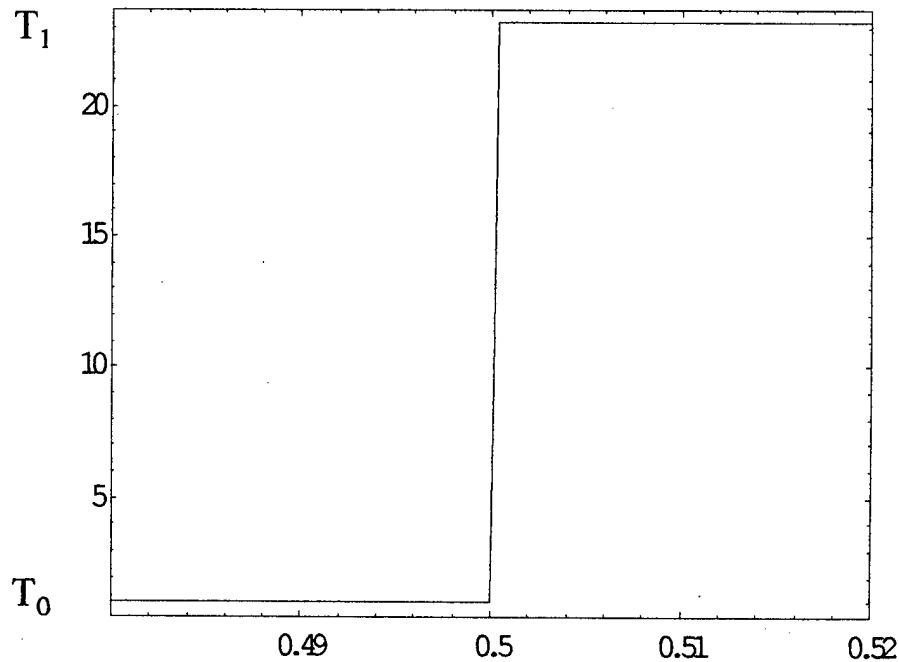
Figure 12. Flux corrected stationary shock.

Modeling the magnetopause as a stationary tangential discontinuity proved

impossible using a one dimensional code. The difficulty in modeling the magnetopause

in a flowing plasma, using a one dimensional algorithm, arises from the violation of the

conservation of mass flux at the tangential discontinuity where the flow velocity must be

equal to zero. Conservation of mass flux states simply that the amount of mass flowing

into a model bin must exactly equal the amount exiting from the opposite side—what

comes in must go out. In a two or three dimensional model this difficulty does not exist:

if the x component of velocity goes to zero, then the y and z velocity components

increase to maintain conservation of mass flux by carrying away mass that would otherwise build up in the system.

To overcome the difficulty of simulating interactions involving a stationary magnetopause using a one-dimensional code, the problem was broken up into two steps. The first step numerically solved the ISW-bow shock interaction separately, with the magnetopause removed from the problem, for the velocities of the two new shock waves S_3 and S_4. Taking the magnetopause out of the model does not affect the behavior S_3 or S_4 because shock waves travel supersonically and are unaffected by changes in fluid conditions upstream.

The second step was to numerically solve the fluid equations for the interaction of S_4 with a tangential discontinuity in a magnetosheath where the flow velocity is zero. It is relatively easy to maintain a stationary discontinuity in a fluid at rest because the mass, momentum, and energy fluxes, $\rho\, u$, $\rho\, u^2$, and $e\, u$ respectively, are zero and are identically conserved. All that is required is to vary temperature, density, and magnetic field in such a way that total the pressure is conserved across the discontinuity, ensuring that a pressure gradient will not form at the boundary and induce the fluid to begin moving. The propagation of S_4 is unaffected when the upstream plasma is at rest because the Mach number, M_4, and hence the propagation speed *relative to the plasma*, depends on the shock strength or the compressibility (Equations (12) or (11) for the gas-dynamic case, Equations (20) or (19) for the MHD case). Propagation speeds in the absolute reference frame will differ by only a constant from the speed in the fluid reference frame.

60

4.2. Model Validation

Having developed a numerical algorithm for a one-dimensional, explicit, time dependent solution of the MHD fluid conservation equations, the algorithm was tested against known analytical solutions to see if it would behave as expected.

The first test was the most straightforward: a simple gas-dynamic Mach 3.5 shock propagating through a plasma at rest. In this test the unshocked upstream plasma was characterized by the ambient solar wind parameters for pressure, density, and temperature listed in Table 1. The analytic solution for the normalized shock propagation speed in terms of Mach number and sound speed is,

$$V = \frac{M a_0}{V_{th}}$$

(73)

where,

$V \equiv$ shock propagation speed,

$M \equiv$ shock Mach number,

$a_0 \equiv$ solar wind sound speed,

$V_{th} \equiv$ solar wind thermal velocity $= (k\, T_0/m)^{1/2}$.

The analytic solution is normalized to the solar wind thermal velocity, V_{th}, to be consistent with the normalization of model parameters (see parameter transformations, page 47). For a Mach 3.5 shock propagating in a stationary solar wind having a sound speed of 33 km/sec and normalized to a thermal velocity of 18 km/sec (from Table 1), Eq (73) yielded a shock speed of 6.3901, shown as the horizontal line in Figure 13.

Positions for the same Mach 3.5 shock wave were determined numerically by the algorithm and were analyzed using a moving average least square fit to the data taken over a twenty-one point interval—ten data points on either side of the point at which the velocity was to be found—in order to estimate shock propagation speeds from the inverse of the linear coefficient of the fitted line. The oscillatory line in Figure 9 is a plot of least-square averaged velocities for the Mach 3.5 shock. The mean averaged shock velocity was 6.3914, agreeing to within less than a tenth of a percent of the analytic solution.
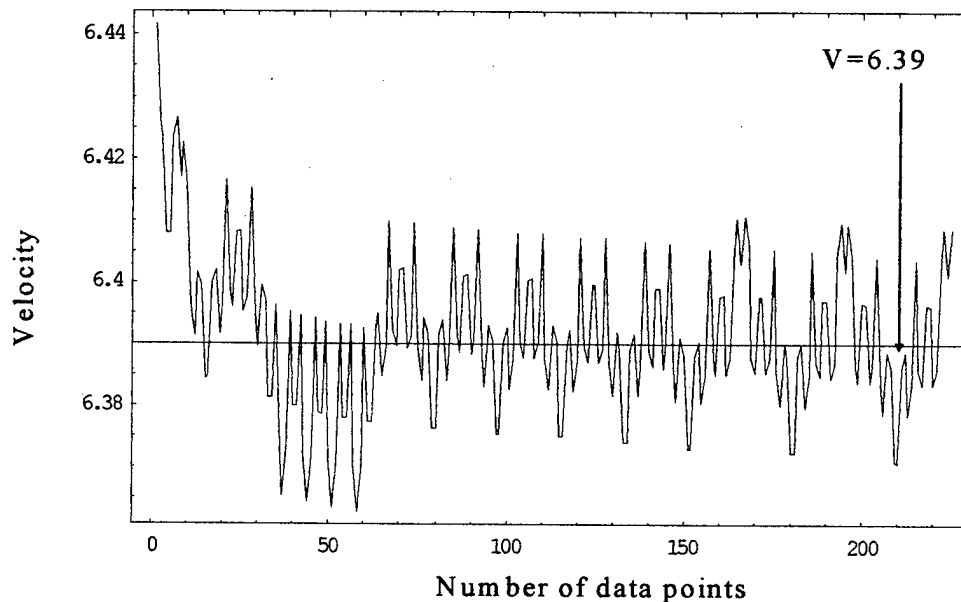
Figure 13. Mach 3.5 shock velocity

The next test was designed to validate the ability of the numerical model to simulate a shock wave-discontinuity interaction. In this case, a Mach 3.5 shock propagating in a stationary gas-dynamic solar wind impinges on a thermal discontinuity. Temperature in the "hot" region was increased by a factor of ten over the solar wind

temperature. To ensure continuity of pressure across the discontinuity, the density was correspondingly decreased to one tenth of the solar wind density. Applying the shock jump equations (Equations (11) - (14)) to a Mach 3.5 shock wave propagating into an unshocked solar wind determined the plasma parameters behind the shock. The plasma parameters for each test region, normalized to ambient solar wind parameters, are presented in Table 4.

Table 4. Gas-dynamic shock-discontinuity validation palsma parameters.

Parameter	Shocked Region	Stationary Solar Wind	Thermalized Region
p	15.06	1.00	1.00
ρ	3.21	1.00	0.10
T	4.69	1.00	10.0
u	4.40	0.00	0.00
a	3.95	1.83	5.77

Recall that a shock impinging on a discontinuity results in a new transmitted shock wave, a reflected rarefaction wave, and a new contact discontinuity as depicted in Figure 5. The Mach number of the transmitted shock, M_6, was determined analytically by first solving the following equation for y_2,

$$\frac{(1-\mu)(y_1-1)}{\sqrt{(1+\mu)(y_1+\mu)}} - \frac{2}{\gamma-1}\left[\left(\frac{y_2}{y_1}\right)^{(\gamma-1)/2\gamma} - 1\right]\left(y_1 \frac{1+\mu+y_1}{\mu+y_1}\right)^{1/2} = \sqrt{\frac{\rho_1}{\rho_2}} \frac{(1-\mu)(y_2-1)}{\sqrt{(1+\mu)(y_2+\mu)}} \quad (74)$$

with,

$$\mu \equiv (\gamma-1)/(\gamma+1),$$

$y_2 \equiv$ shock strength in the thermalized region,

$y_1 \equiv$ shock strength of the shock in the solar wind,

$\rho_1 \equiv$ density in the solar wind,

$\rho_2 \equiv$ density in the thermalized region (Wright, 1961:79);

and then by setting y_2 equal to the gas-dynamic shock strength (Eq (12)). With M_6 known, the speed of the transmitted shock, V_6, was then found from Eq (73), and the flow speed behind the transmitted shock, u_6, was easily solved using Eq (13). Flow velocity behind the transmitted shock is of interest because it is the speed at which the contact surface will move.

The numerical algorithm was executed for a Mach 3.5 shock propagating in a stationary solar wind plasma in which the same thermal discontinuity—i.e. $T = 10.0\ T_0$ and $\rho = 0.1\ \rho_0$ —was initialized. The model tracked the positions of the transmitted shock and the contact discontinuity, but failed to locate the rarefaction wave, except perhaps at the onset of the modeled interaction, as illustrated by the x-t plot of shock position data. The locator subroutine failed to detect the rarefaction wave because changes in density are spread out over many bins, thus decreasing density gradients within the wave below the locator threshold criteria.
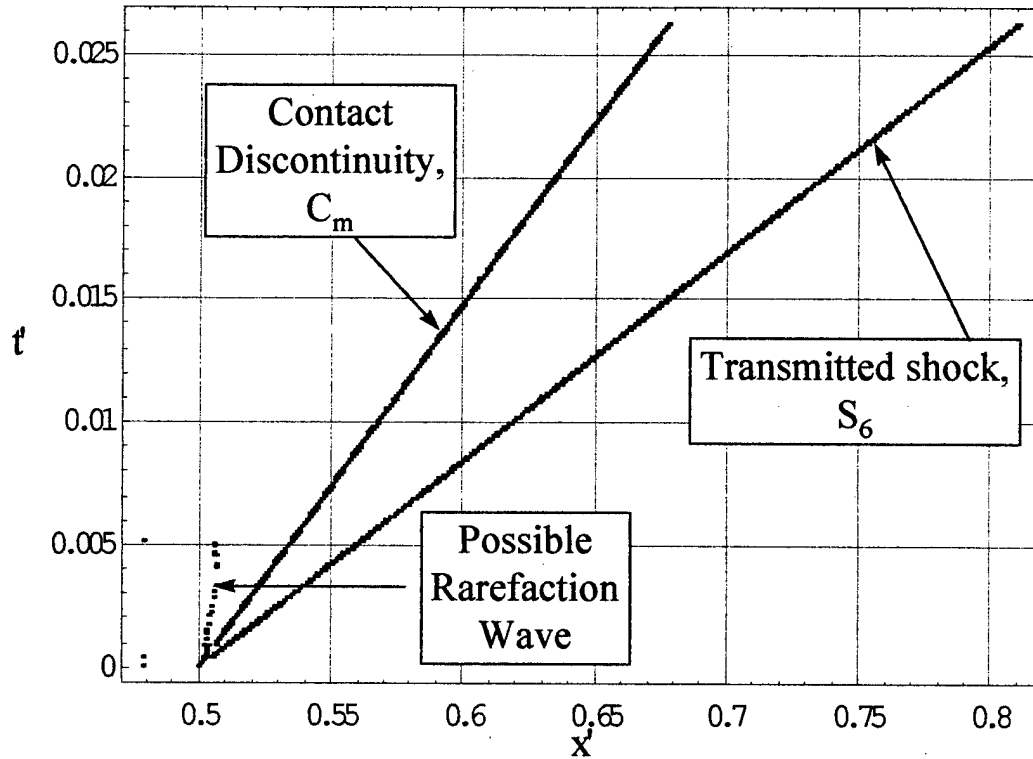
Figure 14. Shock-discontinuity x-t diagram.

Analytic and numerical mean averaged velocities for M_6 and u_6 are shown in Table 5.

Again the numerical model was within less than a percent of the analytical solution.

Table 5. Gas-dynamic shock-discontinuity validation results.

Speed	Analytic Results	Numerical Result	% Error
V_6	11.82	11.84	-0.17
u_6	6.752	6.800	-0.71

The last test of the model using the gas-dynamic governing fluid equations is a

shock-shock interaction representing the ISW-bow shock collision. Here a Mach 3.5

interplanetary shock propagating through a solar wind flowing at 280 km/sec impinges on

a stationary bow shock resulting in two shock waves, S_3 and S_4, with a contact

discontinuity, C_1, between them. Initial normalized plasma parameters are given in Table 6.

Table 6 . Gas-dynamic shock-shock validation plasma parameters.

Parameter	Shocked Region	Solar Wind	Magnetosheath Region
p	15.06	1.00	88.70
ρ	3.21	1.00	3.84
T	4.69	1.00	23.11
u	19.80	15.40	4.01
a	3.95	1.83	8.78

Grib's equations (Equations (39) and (40)) describing the continuity of flow velocity and pressure across C_1 are solved simultaneously to obtain values for M_3 and M_4: 3.60 and 1.54 respectively. The propagation speeds of S_3 and S_4, V_3 and V_4, are found after substituting M_3 and M_4 into Eq (73), and Eq (35) with M_3 results in a determination of the speed u_3, and thus the speed of C_1.

The analytic and numerical solutions for the velocities of the shock waves and the contact discontinuity are presented in Table 7.

Table 7. Gas-dynamic shock shock validation results.

Speed	Analytic Result	Numerical Result	% Error
V_3	5.55	5.60	0.90
V_4	17.57	17.86	1.65
u_3	9.92	9.91	0.10

After demonstrating the ability of the algorithm to produce reasonable

approximations of shock interactions consistent with analytic solutions for a gas-dynamic

plasma, the next step in the validation procedure was to repeat the tests to show that the

model also reasonably approximated shock interactions and movement for a MHD

plasma. As in the validation of the gas-dynamic model, the first test of the MHD

algorithm was to compare the numerical solution for a Mach 3.5 shock wave propagating

through a stationary solar wind plasma and compare the result to the expected analytical

result, $V=6.3900$, obtained from Eq (73). Analysis of the numerical data yields a mean

averaged velocity of 6.39104, within 0.016% of the analytic value.

Following the same procedure that was used to validate the gas-dynamic

algorithm, the next test of the MHD model was an attempt to simulate a shock-

discontinuity interaction within a stationary solar wind plasma. The attempt to model the

Mach 3.5 shock-discontinuity interaction failed. An attempt was made to substitute a

Mach 1.5 shock in the problem with similar results. A last attempt to achieve positive

results involved switching to a Mach 8.0 shock propagating through a *magnetosheath*

plasma in pressure balance with a more realistic magnetopause. Plasma parameters for

the magnetosheath and magnetosphere used in this simulation are listed in Table 8.

Table 8. MHD magnetosheath and magnetopause parameters.

Parameter	Region 1	Magnetopause
Density , ρ (x 10^{-20} kg/m^3)	6.85	0.68
Temperature, T (x 10^4 °K)	88.6	8.86
Flow Velocity, u (km/sec)	75.0	0.00
Magnetic Field, B (nT)	13.1	51.6
Pressure, P (x 10^{-11} Pa)	1.08	0.01
Sound Speed, a (km/sec)	156	49.4
Plasma Beta	14.8	0.009

Parameters in Table 8 are chosen to be consistent with Grib's treatment of the magnetopause.

The Mach 8.0 simulation succeeded in resolving a transmitted shock, a contact discontinuity, and suggestions of a rarefaction wave from location data, but velocity approximations from the model differed significantly (~ 14-20%) from analytic solutions. The result of the Mach 8.0 simulation are given in Table 9 along with analytic solutions and solutions from Grib (1979:5912) of a similar calculation. The analytic solutions were derived from the MHD continuity of plasma flow velocity and total pressure (Equations (45) and (46)) for a stationary solar wind plasma with a magnetic field of 3.5 nT. Grib applies the same continuity equations to a solar wind plasma in which the magnetic field is 2.5 nT (1979:5912).

Table 9. MHD shock-discontinuity validation results.

Speed	Analytical Solution	Numerical Results	Grib's Solution
V_6	16.04	18.35	15.69
u_6	8.88	10.66	12.55

The failure of the model to simulate the shock-discontinuity interaction for the MHD plasma is disturbing. However, failure in this one particular simulation should not be taken as evidence that the model does not reasonably approximate these kinds of interactions, especially in light of other successful simulations of shock wave propagation and shock-shock interactions. It is, rather, an indication that further work is

needed to refine the representation of a stationary discontinuity and the equations that determine the analytic solutions.

On a positive note, the last simulation to test the ability of the model to simulate shock-shock interactions in a MHD fluid was successful. A Mach 3.5 shock was propagated into a non-stationary solar wind plasma flowing at 280 km/sec and allowed to collide with a stationary bow shock. The model handled this particular simulation very well. The location of each of the resultant shock wave pair, and the contact discontinuity between them, was tracked quite effectively by the program as seen in the figure below.
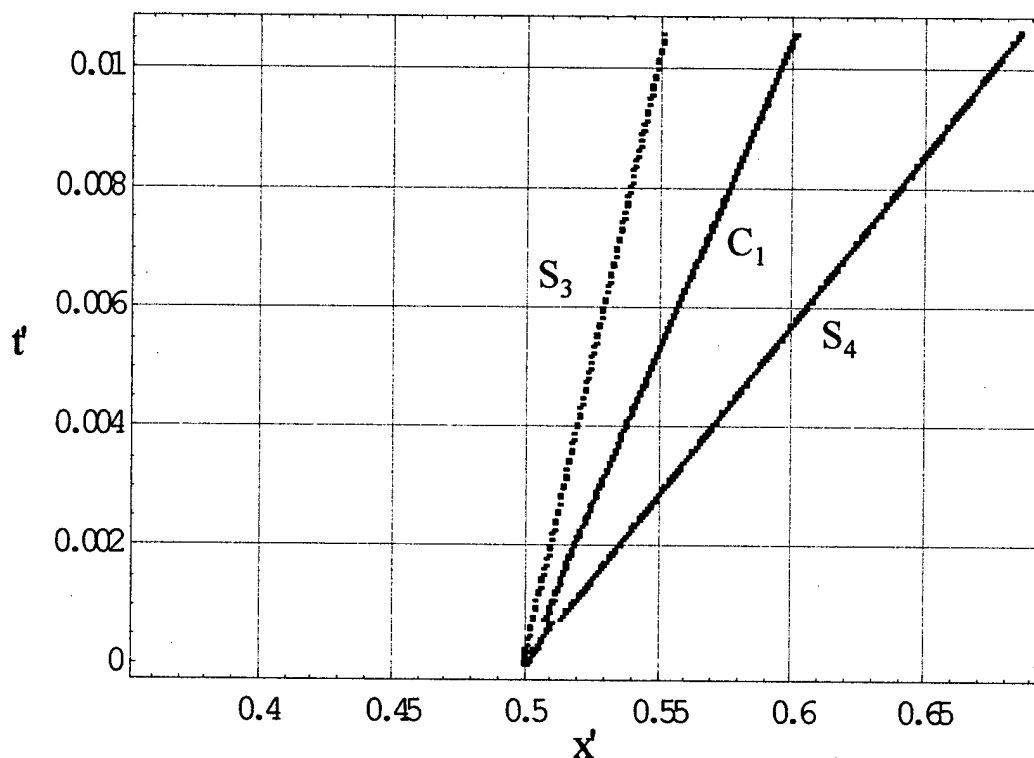

Figure 15. Numerical shock-shock interaction.

The analytic solutions for shock speed were derived as before: the equations of continuity of flow velocity and total pressure (Equations (45) and (46)) across the contact discontinuity C_1 were solved simultaneously to determine M_3 and M_4. The upstream flow into S_3 is a plasma previously shocked by the initial Mach 3.5 shock wave; the upstream sound speed, a_2, is found by applying the shock jump equations (Equations (19) - (23)) with $M = 3.5$ to solar wind parameters and then substituting the resultant pressure and density into equation (2). Similarly, the sound speed upstream from S_4 is just the magnetosheath sound speed and Eq (73), applied to the two new shock waves results in the normalized propagation speeds. The speed of C_1 is the flow speed of the plasma between the two shocks determined by either the left or right sides of Eq (43). The analytical solutions are shown with the numerical results in Table 10.

Table 10. MHD shock-shock validation results.

Speed	Analytic Results	Numeric Results	% Error
V_3	5.15	4.89	5.07
V_4	17.32	17.58	1.50
u_3	9.45	9.59	1.48

Comparing the results presented in Tables 7 and 10 for the gas-dynamic and MHD solutions of the shock-shock interactions it is seen that magnetic effects within the model slowed V_4 and V_3 slightly (by ~ two percent and twelve percent respectively, in this case), and slightly increases the velocity of the contact discontinuity. This observation is consistent with Shen's estimate that the magnetic field slowed the propagation speed of S_4 and S_3 by about ten percent (Shen and Dryer, 1972:4635).

4.3 Model Initialization and Execution

The final section in this chapter is a discussion of the methodology of model initialization , execution, and data processing. Plasma pressure, density, temperature, magnetic field (for MHD fluids only), and flow velocity must be initialized by the user at each bin in the numerical model. In addition, each parameter must be normalized to an ambient, unshocked plasma determined from number density, temperature, magnetic field, and flow velocity supplied by the user as input to the model. The program assists in the initialization process by determining appropriate normalized parameters for the bow shock and ISW based upon the shock jump equations and a Mach number for the ISW, which is also provided by the user, but parameter values at each bin must be set manually from inside the code. Other input variables used by the algorithm include the scale length of the physical problem and the number of bins desired, which determines the spatial size of the grid. The user selects a termination criteria: a specified number of iterations, or at a specified end time. Initial locations in normalized x coordinates of the ISW, bow shock and magnetopause are also input by the user.

The input parameters n_0, T_0, B_0, and M_2 used to validate the model were selected to coincide with Grib, et. al. In their paper, they chose three values for the incident shock wave Mach number, $M_2 = 1.5$, 3.5, and 8.0, as a representative range from low to high values.

Once the model was initialized, execution proceeded fairly quickly on a desk top computer. Typical execution times were about 5 - 20 minutes depending on the size of

the grid and the speed of the shock wave simulated. Large grid sizes produced large data files and a disproportionate time was spent writing to output. A gut feel choice was made to adopt a 2401 (it must be an odd number) bin grid as a compromise between fine spatial resolution and long simulation times, and a coarse grid with a fast execution time that might not spatially resolve shock fronts or density discontinuities. Strong shocks with a high Mach number, >5, propagate quickly across a model bin, requiring a very short time step in order to prevent flow across more than one model bin. A shorter step time increased both computation time and data storage requirements.

The ability to process data files generated by the model into x-t diagrams, and into pressure, density, temperature, and velocity profiles that could then be animated to show the time evolution of the numerical simulation was a useful tool to understand both the physical and numerical processes.

The development and validation of an algorithm to numerically solve the one-dimensional gas-dynamic and MHD fluid equations, and extraction of shock velocities and locations from the output data, has demonstrated the applicability and utility of this analysis tool to the investigation of bow shock and magnetopause displacement resulting from an impinging interplanetary shock wave. In the next chapter the results of the application of the algorithm developed here will be presented and discussed.

V. Results

This chapter is a presentation of the results of a systematic application of the numerical algorithm developed in this thesis to the problem of determining initial bow shock and magnetopause displacement following interaction with an interplanetary shock wave. For both the gas-dynamic and the MHD cases, three incident interplanetary shocks—having Mach numbers $M_2 = 1.5, 3.5$, and 8.0—were simulated interacting with the earth's bow shock. The algorithm was also applied to the interaction of the magnetopause with three different shock waves, S_4, resulting from the ISW-bow shock collision. Numerical solutions for shock and discontinuity velocities, derived from data resulting from these simulations are presented for comparison with normalized analytic velocities determined from the application of the appropriate forms of the equations of continuity across contact discontinuities and Eq (73).

The first set of results are from the gas-dynamic and MHD simulations of the ISW-bow shock collision. The ambient plasma in the these simulations was the quiet solar wind flowing at 280 km/sec, in which a stationary bow shock was maintained. The normalized results are presented in tabular form in Tables 11 and 12. A small xx in the tables indicates missing data due to the failure of the locator subroutine to detect small gradients in the output data. The symbol $\Delta\%$ represents the percentage error between the "true" analytic and the time-averaged numerical solutions, defined by,

$$\Delta\% = \frac{\text{Analytic} - \text{Numeric}}{\text{Analytic}} \times 100.$$

Table 11. Gas-dynamic shock-shock results.

Incident Mach Number	Type Solution	V_3	V_4	u_3
$M_2 = 1.5$	Analytic	2.32	14.30	6.14
	Numerical	2.29	14.32	6.05
	$\Delta\%$	1.29	-0.14	1.47
$M_2 = 3.5$	Analytic	5.55	17.57	9.94
	Numerical	5.60	17.86	9.91
	$\Delta\%$	-0.90	-1.65	0.30
$M_2 = 8.0$	Analytic	7.51	22.73	14.97
	Numeric	7.49	23.96	14.51
	$\Delta\%$	0.26	-5.41	-3.10

Table 12. MHD shock-shock results.

Incident Mach Number	Type Solution	V_3	V_4	u_3
$M_2 = 1.5$	Analytic	2.24	14.30	6.06
	Numerical	-1.4	11.45	2.01
	$\Delta\%$	162	20	66.8
$M_2 = 3.5$	Analytic	5.15	17.34	9.89
	Numerical	4.89	17.57	9.58
	$\Delta\%$	5.04	-1.32	3.13
$M_2 = 8.0$	Analytic	7.50	22.75	14.83
	Numeric	7.31	22.88	14.64
	$\Delta\%$	2.53	-0.57	1.28

74

Tables 11 and 12, show that the algorithm closely approximated the velocities determined by the analytic equations for V_3 and V_4 to within about five percent in all but one simulation. An analysis of shock positions from the MHD simulation of the $M_2 = 1.5$ shock indicated a negative value for V_3 and a lower value of V_4. Movement of S_3 in the negative (left) direction indicates that the propagation speed, $V_3 = M_3 a_2$, of the new bow shock into the upstream ISW plasma is greater than the flow velocity u_2 since, in the rest reference frame, shock propagation speed is determined by $u_2 - V_3$; this problem could arise if the solar wind flow velocity, u_0, was mistakenly set to zero in the numerical model. A stationary solar wind would also explain propagation speeds for C_1 and V_4 less than analytical predictions because the magnetosheath flow velocity depends on the solar wind flow speed from the shock jump equations—zero magnetosheath flow speed translates into slower than expected V_4 and u_3.

The second set of data presented are the result of gas-dynamic simulations of the S_4-magnetopause interaction. Because S_4 results from the interaction of the ISW with the bow shock, to properly initialize the model required prior determination of M_4, and all plasma parameters associated with the shock, using the equations of continuity for flow velocity and pressure and the shock jump equations. In this simulation, magnetospheric plasma density was assumed to be one-tenth the density in the magnetosheath, consistent with Grib's analysis; to maintain a balance of pressure across the tangential discontinuity, a magnetospheric temperature equal to ten times the magnetosheath temperature was required.

The Mach number for the transmitted shock, M_6, was determined from Grib's

equations for continuity of flow velocity and pressure (Equations (39) and (40)) across

the new magnetopause, C_m. Because the plasma was assumed to be an adiabatic ideal

gas, a_5 and p_5, the sound speed and pressure in the rarefaction wave, had the forms of

Equations (41) and (42). M_6 and a_m, the magnetospheric sound speed determined by the

initialization of the magnetosphere, determined the shock speed when substituted into Eq

(73).

Table 13. Gas-dynamic shock-discontinuity results.

Incident Mach Number	Type Solution	V_6	u_6
$M_2 = 1.5$	Analytic	30.00	3.18
	Numerical	29.96	3.19
	$\Delta\%$	0.007	-0.063
$M_2 = 3.5$	Analytic	34.37	8.97
	Numerical	34.43	8.98
	$\Delta\%$	-0.19	-0.15
$M_2 = 8.0$	Analytic	41.01	16.67
	Numeric	41.05	16.70
	$\Delta\%$	-0.11	-0.20

The last set of results presented are the from the $M_2 = 8.0$ MHD simulations of

the S_4-magnetopause interaction shown in Table 14. Again, the large discrepancies

between analytical and numerical solutions, and the lack of usable data for the $M_2 = 1.5$

and 3.5 simulations suggest a flaw in the numerical code to model the magnetopause in a

MHD plasma, errors in the analytic solutions, or a combination of both.

Table 14. MHD Mach 8.0 shock-discontinuity results.

M = 8.0 Results	Type Solution	V_6	u_6
Analytic	Analytic	16.04	8.88
	Numerical	18.35	10.66
	$\Delta\%$	-14.4	-20.0
Grib	Grib	15.69	12.55
	Numerical	18.35	10.66
	$\Delta\%$	-17.0	15.1

The good agreement between analytic and numerical solutions for velocities of the two new shock waves resulting from collision of an interplanetary shock wave and the earth's bow shock, as well as the gas-dynamic solutions to the shock-discontinuity interaction, suggests that the algorithm developed in this thesis is sound. Though discouraging, the failure of the algorithm to closely approximate the analytical results for the MHD shock-magnetopause simulations indicate a need for refinement of the analytic solutions to eliminate possible errors, and of the initialization of plasma parameters put into the model to represent the magnetopause. These results show that the algorithm produces reasonable approximations to plasma behavior consistent with an analytic analysis, primarily by Grib, et. al., which describe the physical processes modeled in these simulations: a logical next step is a thorough validation of the model with respect to real observations of the bow shock and magnetopause motions. The kind of validation required is becoming more feasible as the number of space platforms and observation techniques continues to expand the database of bow shock and magnetopause behaviors.

VI. Conclusions and Recommendations

This thesis had four objectives. The first was to develop an understanding of the physical processes associated with the displacement of the earth's bow shock and magnetopause initiated by collision of an ISW with the magnetosheath system. The second objective was the development of a one-dimensional numerical simulation of the ISW-magnetosheath interactions based upon gas-dynamic and MHD fluid equations to determine the displacements and velocities of the bow shock and the magnetopause. A third objective was to review and understand prior analytic treatments of the ISW-magnetosheath interactions, providing a basis for comparison with numerical results. And the fourth objective was to evaluate the performance of the numerical model by comparing simulation results with analytic solutions. In terms of development and validation of an algorithm to solve the one-dimensional fluid equations, and the application of the algorithm to simulations of the ISW-magnetosheath interactions, this thesis has accomplished each of its objectives.

Based on the validation of the algorithm and simulations of the ISW-bow shock interactions, the development of the governing fluid equations and their incorporation into a numerical algorithm to model these interactions is sound. A problem simulating the shock-magnetopause interactions does not cast doubts on the basic soundness of the model; it does indicate that the MHD treatment of the shock-magnetopause interaction requires further development.

During the course of this thesis project, several ideas aimed to improve the model and enhance its utility in the simulation of bow shock and magnetopause interaction were developed and are presented as recommendations to those interested or who may wish to continue this work.

The first recommendation is to expand the one dimensional model into a two or three dimensional code in order to better simulate the entire interaction of an ISW with the magnetosheath system. A multidimensional code would permit a seamless simulation without the necessity of dividing the problem into two separate steps. A multidimensional code would also allow a more realistic simulation of a magnetosheath in which the flow velocity at the stagnation point equaled zero without violating the conservation of mass, momentum, and energy fluxes. A seamless simulation of the ISW-magnetosheath interactions would conceivably permit numerical simulation of multiple rarefaction wave reflections between the advancing bow shock and magnetopause which are proposed by Grib, et. al. as the mechanisms that eventually slow and reverse the magnetopause during magnetospheric compression.

A second recommendation is that the initialization of the magnetosphere in the model be verified and corrected if necessary, and that the simulations of the shock-magnetopause interactions be re-accomplished.

A third, and final, recommendation is that this algorithm be validated, as the data becomes available, by comparison of numerical solutions to observations of actual bow shock and magnetopause displacements. The validation may suggest ways that the

algorithm can be improved or applied to other problems of interest in plasma or shock physics.

VII. Bibliography

Courant, R. and K.O. Friedrichs. Supersonic Flow and Shock Waves. New York: Interscience Publishers, 1948.

Fletcher, C.A.J. Computational Techniques for Fluid Dynamics. Vol. II: Specific Techniques for Different Flow Categories, 2d ed. Berlin: Springer-Verlag, 1991.

Grib, S.A., et. al. "Interaction of Interplanetary Shock Waves with the Bow Shock-Magnetopause System," Journal of Geophysical Research, 84, No. A10:5907-5921 (October, 1979).

Hilbun, W. A One Dimensional MacCormack Algorithm with FCT, Unpublished software, Air Force Institute of Technology, Dayton (1997).

Hudson, M.K., et. al. "Simulation of Proton Radiation Belt Formation", Geophysical Research Letters, 20 N0. 3:291-294 (February, 1995).

Kivelson, M. and C. Russell. Introduction to Space Physics. New York: Cambridge, 1995.

Landau, L. D. and E. M. Lifshitz. Fluid Mechanics. London: Pergamon Press, 1959.

Li, Xinlin, et. al. "Simulation of the Prompt Energization and Transport of Radiation Belt Particles During the March 24, 1991 SSC," Geophysical Research Letters, 20, No. 22:2423-2426 (November, 1993).

Parks, George K. Physics of Space Plasmas: An Introduction. New York: Addison-Wesley, 1996.

"SOHO Orbit Schematic." Excerpt from the SOHO Home Page, n. page. WWWeb http://sohowww.nascom.nasa.gov/gif/halo_orbit.gif. 6 November, 1997.

Tascione, T. F. Introduction to the Space Environment, 2d ed. Malabar: Krieger Publishing, 1994.

Tóth, G. and D. Odstr̃il. "Comparison of Some Flux Corrected Transport and Total Variation Diminishing Numerical Schemes for Hydrodynamic and Magnetohydrodynamic Problems," Journal of Computational Physics, 128,:82-100 (1996).

Shen, W.W. "Interaction of Interplanetary MHD Shock Waves with the Magnetopause," Astrophysics and Space Science, 24:51-64 (February, 1973).

Shen, W.W. and M. Dryer. "Magnetohydrodynamic Theory for the Interaction of an Interplanetary Double-Shock Ensemble with the Earth's Bow Shock," Journal of Geophysical Research, 77, No. 25:4627-4644 (September, 1972).

Vvedensky, D. D. Partial Differential Equations With Mathematica. London: Addison-Weseley, 1993.

Wright, J.K. Shock Tubes. London: Methuen, 1961.

Vita

Capt William A. Olson was born on 13 October 1963 in Tooele, Utah. He graduated from Tooele High School in 1982 and entered undergraduate studies at Brigham Young University in Provo, Utah in August 1984. Upon graduation in 1988 with a Bachelor of Science degree in Physics, he entered Officer Training School in San Antonio, Texas and was commissioned a 2nd Lieutenant in May 1989. For the next year he attended the University of Oklahoma in Norman, Oklahoma where he completed the Basic Meteorology Program in May 1990.

Capt Olson's first assignment began in June 1990 attached to the XVIII Airborne Corps at Fort Bragg, North Carolina as a Staff Weather Officer (SWO). After completing parachute training, Capt Olson was sent to Saudi Arabia as part of Operations Desert Shield and Desert Storm where he served with the XVIII Airborne Corps and the 24th Infantry Division (Mechanized) in northern Saudi Arabia and southern Iraq. Following the Gulf War he returned to Fort Bragg to serve as XVIII Airborne Corps and 82nd Airborne Division SWOs until 1993.

In February 1993 Capt Olson was reassigned to US Central Command at MacDill AFB, Florida. While at MacDill AFB, he earned a Master of Aeronautical Science degree in Management from Embry-Riddle Aeronautical University. In May 1996 he entered the School of Engineering Physics, Air Force Institute of Technology.

Permanent Address: 606 N Broadway Ave
                    Tooele, UT 84074

REPORT DOCUMENTATION PAGE		*Form Approved* *OMB No. 0704-0188*

Public reporting burden for this collection of information is estimated to average 1 hour per response, including the time for reviewing instructions, searching existing data sources, gathering and maintaining the data needed, and completing and reviewing the collection of information. Send comments regarding this burden estimate or any other aspect of this collection of information, including suggestions for reducing this burden, to Washington Headquarters Services, Directorate for Information Operations and Reports, 1215 Jefferson Davis Highway, Suite 1204, Arlington, VA 22202-4302, and to the Office of Management and Budget, Paperwork Reduction Project (0704-0188), Washington, DC 20503.

1. AGENCY USE ONLY *(Leave blank)*	2. REPORT DATE DEC 97	3. REPORT TYPE AND DATES COVERED MASTER'S THESIS

4. TITLE AND SUBTITLE DISPLACEMENT OF THE EARTH'S BOW SHOCK AND MAGNETOPAUSE DUE TO AN IMPINGING INTERPLANETARY SHOCK WAVE	5. FUNDING NUMBERS
6. AUTHOR(S) William A. Olson, Captain, USAF	

7. PERFORMING ORGANIZATION NAME(S) AND ADDRESS(ES) Air Force Institute of Technology 2750 P Street Wright-Patterson AFB, OH 45433-7765	8. PERFORMING ORGANIZATION REPORT NUMBER AFIT/GAP/ENP/97D-08

9. SPONSORING/MONITORING AGENCY NAME(S) AND ADDRESS(ES) PL/GPS Hanscom AFB, MA 01731-5000	10. SPONSORING/MONITORING AGENCY REPORT NUMBER

11. SUPPLEMENTARY NOTES

12a. DISTRIBUTION AVAILABILITY STATEMENT Approved for public release; distribution unlimited	12b. DISTRIBUTION CODE

13. ABSTRACT *(Maximum 200 words)*

Interplanetary shock waves (ISWs) propagating through the solar wind can "collide" with the earth's bow shock, resulting in a series of new shocks, contact discontinuities, and rarefaction waves which interact to effectively move the bow shock and magnetopause toward the earth. A one-dimensional MacCormack predictor-corrector algorithm with Flux Corrected Transport (FCT) was developed to model the ISW-bow shock and magnetopause interactions, and to numerically predict their propagation speeds after collision. Analytic relationships for the Mach numbers and propagation speeds of the generated shock waves and contact discontinuities were used to validate the model and to compare numerical results. In both the gas-dynamic and magnetohydrodynamic (MHD) fluid approximaitons the model predicted propagation speeds of the moving bow shock to within five percent of analytical solutions. Propagation speeds of the moving magnetopause were also determined to within five percent.

14. SUBJECT TERMS Bow Shock, Magnetohydrodynamics, Shock Waves, Plasma Waves, Space Environment	15. NUMBER OF PAGES 92 ~~85~~
	16. PRICE CODE

17. SECURITY CLASSIFICATION OF REPORT UNCLASSIFIED	18. SECURITY CLASSIFICATION OF THIS PAGE UNCLASSIFIED	19. SECURITY CLASSIFICATION OF ABSTRACT UNCLASSIFIED	20. LIMITATION OF ABSTRACT UL

Standard Form 298 (Rev. 2-89) (EG)
Prescribed by ANSI Std. 239.18
Designed using Perform Pro, WHS/DIOR, Oct 94